Mitigating Adverse Impacts of Negative Damping Induced by Wind Generators on Power Grid Dynamics

Final Project Report

S-69G

Power Systems Engineering Research Center
Empowering Minds to Engineer
the Future Electric Energy System

Mitigating Adverse Impacts of Negative Damping Induced by Wind Generators on Power Grid Dynamics

Final Project Report

Project Team
Ali Mehrizi-Sani, Project Leader
Washington State University

Graduate Student
Hooman Ghaffarzadeh
Washington State University

PSERC Publication 18-01

February 2018

For information about this project, contact:

Ali Mehrizi-Sani
School of Electrical Engineering and Computer Science
Energy Systems Innovation Center (ESIC)
Laboratory for Integration of Power Electronics (LIPE)
Washington State University
EME 35 - 355 NE Spokane Street
Pullman, WA 99164-2752

Power Systems Engineering Research Center

The Power Systems Engineering Research Center (PSERC) is a multi-university Center conducting research on challenges facing the electric power industry and educating the next generation of power engineers. More information about PSERC can be found at the Center's website: http://www.pserc.org.

For additional information, contact:

Power Systems Engineering Research Center
Arizona State University
527 Engineering Research Center
Tempe, Arizona 85287-5706
Phone: 480-965-1643
Fax: 480-727-2052

Notice Concerning Copyright Material

Acknowledgements

We express our appreciation for the support provided by PSERC industry members. In particular we wish to thank our industry advisors, Dr. Saman Babaei and Mr. Alan Ettlinger from New York Power Authority (NYPA).

We also thank Dr. Dharshana Muthumuni (Manitoba HVDC Research Centre) for the support toward this project, for discussions about PSCAD/EMTDC software tool, and for sharing benchmark system case files.

Executive Summary

In recent years, due to high demand for electrical energy and limited fossil fuel resources, penetration of renewable energy resources into the power grid has increased significantly. Wind, as a renewable and abundantly available source of energy, has an important share in the energy mix for moving away from conventional generation toward renewable generation. In the last decade, the installed global wind power capacity has increased exponentially. About 5.5% of the U.S. generated electrical energy in year 2016 came from the wind power. However, factors such as low fossil fuels prices, grid integration challenges, and lack of public acceptance hinder the penetration of wind power in the power grid.

Subsynchronous resonance (SSR) induced by a wind turbine connected radially through a series-compensated transmission line is one of the major issues related to integration of wind energy in the power system. In SSR, two power system components exchange energy at frequencies below the nominal frequency, which can cause damage to the power system equipment. While conventional RSC and GSC controllers can handle the normal operation of a Type III wind turbine, following a major disturbance (e.g., a fault in the system), the power system may tend toward instability. In such cases, an auxiliary controller can be added to the control loop of the wind turbine to prevent the system instability.

In this project, the multiple-model adaptive control (MMAC) approach is used to propose a supplementary controller to operate in a wide range of operating conditions. In MMAC, a finite number of more probable operating conditions are considered and an appropriate linearized dynamic model is derived for each operating point. The main reason for using a linearized model instead of a nonlinear model is that the design and implantation of a nonlinear control technique is not straight forward.

An MMAC controller has two levels; the first level is a set of controllers designed using standard control methods, and the second level is a supervisory controller that selects the level one controller based on the system conditions. After a change in the operating point of the system, MMAC uses a vector of feedback signals that have the most impact on the output response of the system to identify the best matching model-controller pair for the current operating condition.

The supervisory controller uses a hysteresis algorithm to switch between the controllers in the look-up table. The controllers in the MMAC bank have a similar structure which are connected to the GSC control loop through a washout filter. These controllers are designed using the root-locus tuning method.

While a fixed-parameter controller can operate in a limited operating region, the proposed control technique is shown to provide a significantly better performance for a variable-parameter wind system with a wide operating region. The design and implementation of the proposed control approach is straightforward, and the supplementary controller is added to the existing controllers of the wind turbine. The simulation results show the effectiveness of the proposed supplementary controller to mitigate the subsynchronous oscillations in a wide range of the operating conditions.

Project Publications:

[1] H. Ghaffarzadeh and A. Mehrizi-Sani, "Control techniques for wind energy systems," *IET Renewable Power Generation*, submitted for review, Oct. 2017.

[2] H. Ghaffarzadeh and A. Mehrizi-Sani, "Mitigation of subsynchronous resonance induced by a type III wind turbine," *IEEE Trans. Sustain. Energy*, submitted for review, Feb. 2018.

Student Thesis:

[1] H. Ghaffarzadeh, "System-agnostic controller strategies for renewable energy systems," PhD thesis, Washington State University.

Table of Contents

List of Figures

List of Tables

1. Introduction

1.1 Background

The renewable energy sector in the United States is continuously growing, and wind—an abundantly available source of renewable energy—plays a leading role in this transition [1]: 5.55% of the electrical energy in the United States in 2016 came from the wind [2]. According to the U.S. Department of Energy (DOE), wind energy's contribution to U.S. electricity power generation is expected to increase to 10% by the year 2020, 20% by 2030, and 35% by 2050 [3]. However, factors such as low fossil fuels prices, grid integration challenges, and lack of public acceptance hinder the penetration of wind power in the power grid [4].

1.2 Overview of the Problem

Subsynchronous resonance (SSR) induced by a wind turbine connected to the grid radially (without any other connected lines) through a series-compensated transmission line is one of the major issues related to integration of wind energy [5]. In SSR, two power system components exchange energy at frequencies below the nominal frequency, which can cause damage to the power system equipment [6]. SSR in general can be classified into three categories: (1) subsynchronous torsional interaction (SSTI), (2) subsynchronous induction generator effect (SSIGE), and (3) subsynchronous control interaction (SSCI) [5]. SSTI refers to the interaction between the turbine-generator mechanical parts and the series-compensated transmission line. SSIGE involves the interaction between the generator and transmission line. SSCI is solely an electrical phenomenon related to the wind turbine converter controller and the series capacitor [7].

An example of an SSR event occurred during the commissioning of a 240 MVAr series capacitor on a 345 KV line in the Buffalo Ridge area of Minnesota. Due to wrong switching before bypassing the series capacitor, a line was inadvertently taken out of service. The line outage led to a 150 MW wind farm being radially connected to a 60% series-compensated transmission line. This in turn led to growing subsynchronous currents [8]. As another example, in October 2009, following a topology change due to a single-line-to-ground fault in the ERCOT service area, a Type III wind farm became radially connected to a 50% series-compensated transmission line. The oscillations started immediately after the line outage and fast growing subsynchronous currents and voltages were reported. In a short time, damage occurred in both the wind turbine equipment and the series capacitor [7]. These incidents emphasize the need for a strategy to improve the damping of the system in the presence of compensated line and wind generators.

1.3 Literature Review

Several strategies are introduced in the literature to address this need. Reference [9] studies the application of a STATCOM in damping SSR in a Type III wind turbine. An auxiliary damping control scheme is developed to control the STATCOM and improve the transient stability of the interconnected system. Similarly, [10] evaluates the performance of a STATCOM with a voltage controller at the point of common coupling (PCC) in mitigating SSR in a Type III wind farm. Three different strategies based on FACTS devices are introduced in [6]. In the first two strategies, a GCSC and a TCSC are used to improve damping of the existing controllers in a Type III wind turbine. The third strategy employs an additional fixed-parameter supplementary controller to mitigate SSR. In [11], a supplementary controller using a washout filter, a lead-lag controller, and a band pass filter is developed and added to the reactive power control loop of the grid-side converter (GSC). Similarly, a controller including a gain with phase compensation and a band-pass filter is developed in [12]. Reference [13] demonstrates the capability of a TCSC in damping SSR in a Type III wind farm. For this purpose, an impedance model for the TCSC using dynamic phasor-based modeling approach is developed, and the stability of the system is studied. In [14] the impact of uncertainties on occurrence of SSR in a Type III wind system is discussed and a probabilistic stability analysis is conducted.

The existing supplementary controllers to improve damping of a Type III wind turbine against SSR generally have a simple structure (a controller and a washout filter) and are added to the existing control loops of the Type III converters. However, these controllers have fixed parameters and are not robust against the change of operating condition of the system. The implementation of the FACTS-based approaches is generally expensive and not straightforward.

1.4 Research Objectives

To address the drawbacks of the aforementioned methods, in this project, an adaptive supplementary control strategy using multiple-model adaptive control (MMAC) approach is proposed to mitigate subsynchronous interactions (SSI) induced by a wind turbine connected to a series-compensated transmission line. To evaluate the performance of the controller, small-signal stability of the study system is studied using a comprehensive dynamic model of the wind system. Time-domain simulation results show the effectiveness of the proposed supplementary controller to mitigate subsynchronous oscillations in a wide range of the operating conditions.

1.5 Organization of Report

The rest of this report is organized as follows: Chapter 2 studies SSR in a Type III-based wind system. In Chapter 3 a comprehensive dynamic model of the study system is presented. Chapter 4 introduces the proposed MMAC-based supplementary controller. Chapter 5 presents case studies to evaluate the stability and performance of the proposed strategy. Chapter 6 provides concluding remarks.

2. Subsynchronous Resonance Induced by a Series-Compensated Wind System

2.1 Subsynchronous Resonance

Wind power plants are usually located far from the main grid to take advantage of more favorable wind conditions. A transmission line then transfers the generated electrical energy to the grid. To increase the power transfer capability of this line, it is typically series-compensated. However, radial connection of a Type III-based wind farm to a compensated transmission line increases the risk of SSR and instability [15].

The frequency of the electrical oscillations f_{eo} in a series-compensated system is [7]

$$f_{eo} = \pm f_s \sqrt{\frac{X_C}{X_L}}, \tag{2.1}$$

where f_s is the synchronous frequency (50 or 60 Hz), and X_C and X_L are the reactance of the series capacitor and total reactance of the transmission line, generator, and transformers, respectively [7].

Fig. 2.1 depicts the steady-state equivalent circuit of a doubly fed induction generator (DFIG).

The equivalent rotor resistance $r_{r,\mathrm{eq}}$ and rotor voltage $V_{r,\mathrm{eq}}$ in the steady-state are

$$r_{r,\mathrm{eq}} = \frac{r_r}{s_1} \tag{2.2}$$

$$V_{r,\mathrm{eq}} = \frac{V_r}{s_1}, \tag{2.3}$$

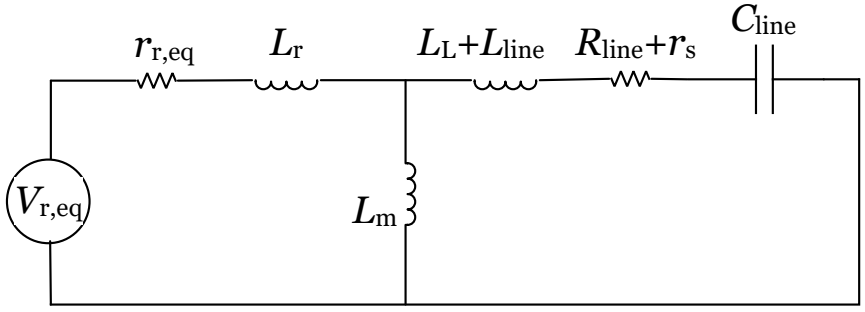

Figure 2.1: Steady-state equivalent circuit of a DFIG.

where slip s_1 at subsynchronous frequency f_{eo} is given by

$$s_1 = \frac{f_{eo} - f_{el}}{f_{eo}}, \tag{2.4}$$

where f_{el} is the electric frequency corresponding to the rotating speed [5]. $r_{r,\text{eq}}$ at subsynchronous frequency is negative, since $f_{eo} < f_{el}$ (or $s_1 < 0$). Therefore, if $|r_{r,\text{eq}}| > |R_{\text{line}} + r_s|$, the system exhibits negative damping and growing subsynchronous oscillations appear in the rotor current [5, 6].

2.2 Classification of Approaches to Mitigate SSR

Different approaches to mitigate SSI include (1) using flexible AC transmission systems (FACTS), (2) bypass filters across the series capacitor, (3) detection algorithms to trip the wind generator, and (4) modification of wind turbine control systems. Modification of wind turbine control systems is the most practical approach because it is economical, avoids generator tripping, does not need installation of expensive additional damping devices (FACTS), and can be quickly implemented. In this project, using this approach, a supplementary adaptive controller is proposed and added to the grid-side converter (GSC) control loop.

2.3 Classification of Wind Turbines

Wind turbine technology has seen a significant progress in recent years and several types of wind turbines are in use [16, 17]. In general, wind turbines can be classified into four types based on their power electronics: (1) fixed-speed (Type I), (2) variable-slip (Type II), (3) doubly fed induction generator (Type III), and (4) full converter (Type IV) wind turbines. Variable-speed wind turbines, i.e., Types III and IV, are currently the most commonly used turbines [1].

According to the JRC database (Joint Research Center of the European Commission), in 2005 40% of the North American total wind power installed capacity was Type I and II and 60% Type III. In 2014, almost 70% of the installed capacity was Type III, 29% Type IV, and less than 1% Types I and II [18]. Fig. 2.2 shows the schematic diagram of Types I, II, III, and IV wind turbines. The focus of this project is on the Types III wind turbine becuase it is currently the most commonly used turbine [1].

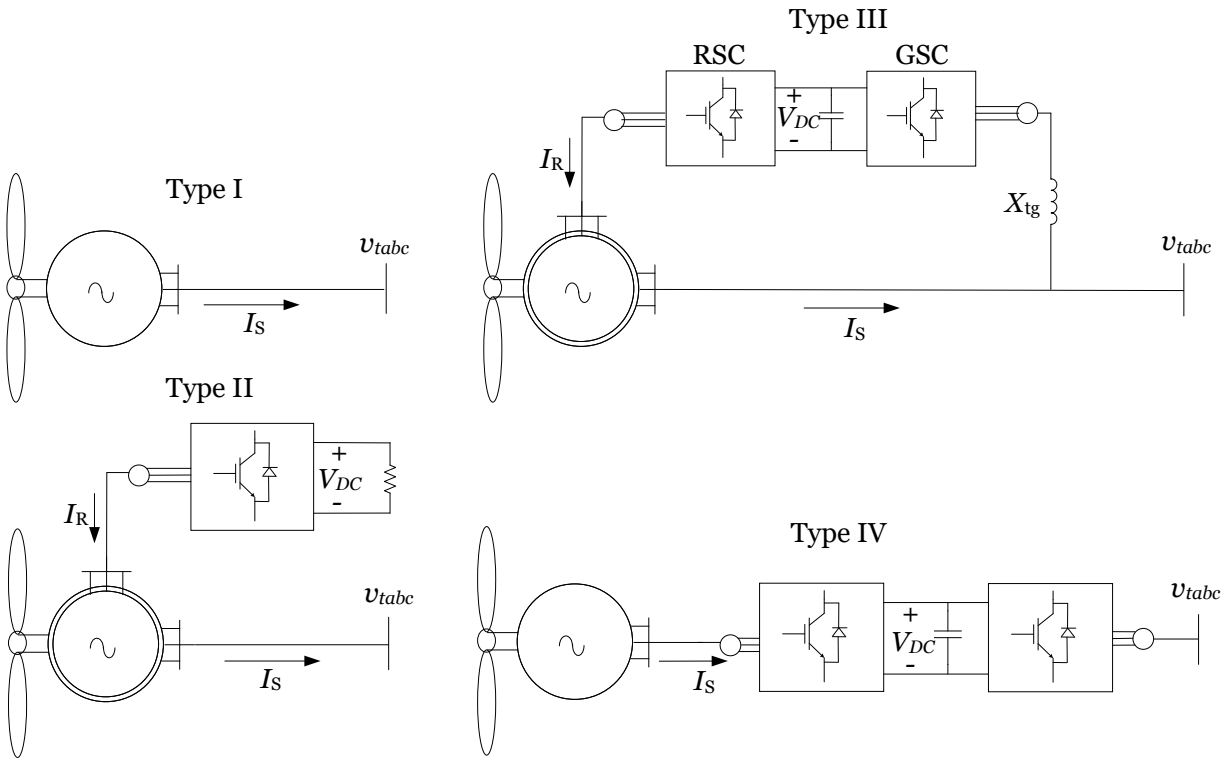

Figure 2.2: Types I, II, III, and IV wind turbines.

3. Dynamic Modeling of a Series-Compensated Type III Wind System

The focus of this project is on the Types III wind turbine becuase it is currently the most commonly used turbine [1]. According to the JRC database (Joint Research Center of the European Commission), in 2014, almost 70% of the installed capacity was Type III, 29% Type IV, and less than 1% Types I and II [18]. The dynamic behavior of a Type III wind turbine can be expressed using a set of subsystems whose are modeled in the *qd*-reference frame as shown in Fig. 3.1:

- Aerodynamics of wind turbine;
- Mechanical shaft system;
- Induction generator;
- Rotor-side and grid-side converters controllers;
- DC-link capacitor; and
- Transmission line.

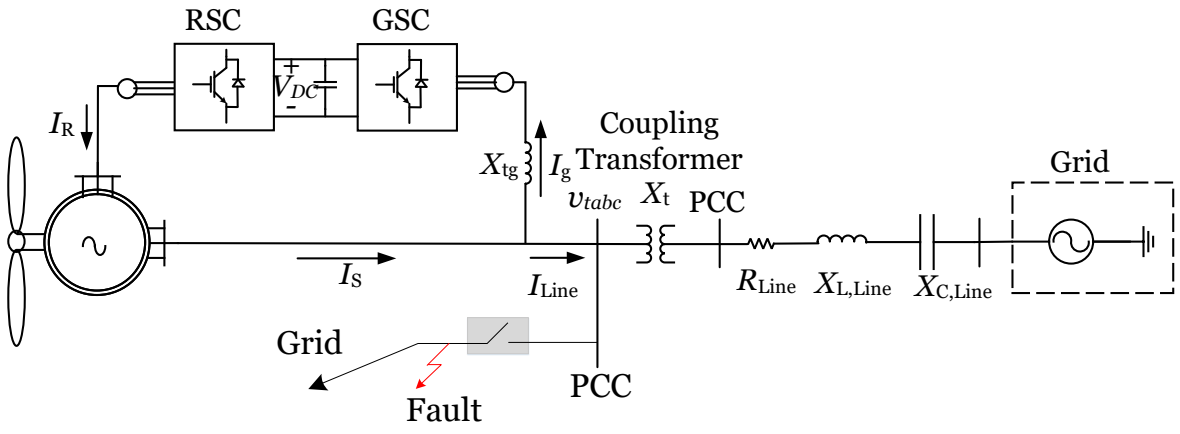

Figure 3.1: Schematic diagram of a Type III wind system.

3.1 Aerodynamics of the Wind Turbine

The turbine mechanical torque can be calculated as

$$T_w = \frac{0.5\rho\pi R^2 C_p V_w^3}{\Omega_m}, \tag{3.1}$$

where V_w is the wind speed, ρ is the air density, R is the rotor radius, Ω_m is the mechanical angular velocity, and C_p is the power coefficient of the blade calculated as

$$C_p = 0.5(\frac{RC_f}{\lambda_w} - 0.022\gamma_w - 2)e^{-0.225\frac{RC_f}{\lambda_w}}, \tag{3.2}$$

where C_f is a blade design constant, γ_w is the pitch angle, and λ_w is the tip-speed ratio defined as [5, 19]

$$\lambda_w = \frac{\Omega_m R}{V_w}. \tag{3.3}$$

3.2 Mechanical Shaft System

Depending on the required accuracy, the dynamic of the shaft system can be represented with the following models: (1) six-mass shaft model, (2) three-mass shaft model, (3) two-mass shaft model, and (4) single-mass or lumped model [20]. Due to the decoupling feature of the AC/DC/AC converter in a Type III wind turbine, the mechanical shaft system properties have an insignificant effect on the grid-side characteristics. In the single-mass lumped model, the whole dynamic of the drivetrain components of a wind turbine is expressed in a single differential equation. However, the two-mass shaft model can provide more accurate representation of the low-speed turbine and the high-speed generator characteristics of a Type III wind turbine [20].

$$\frac{d}{dt}\begin{bmatrix}\omega_t\\ \omega_r\\ T_{tg}\end{bmatrix} = \begin{bmatrix}-\frac{D_t+D_{tg}}{2H_t} & \frac{D_{tg}}{2H_t} & -\frac{1}{2H_t}\\ \frac{D_{tg}}{2H_g} & -\frac{D_g+D_{tg}}{2H_g} & -\frac{1}{2H_t}\\ K_{tg}\omega_b & -K_{tg}\omega_b & 0\end{bmatrix}\begin{bmatrix}\omega_t\\ \omega_r\\ T_{tg}\end{bmatrix} + \begin{bmatrix}\frac{1}{2H_t} & 0 & 0\\ 0 & \frac{1}{2H_g} & 0\\ 0 & 0 & 1\end{bmatrix}\begin{bmatrix}T_w\\ T_e\\ 0\end{bmatrix} \tag{3.4}$$

In (3.4), wind turbine speed ω_t, generator rotor speed ω_r, and internal torque of the two-mass system T_{tg} are the state variables. Wind torque T_w and electric torque T_e are the inputs [21]. T_e is calculated as

$$T_e = \frac{L_m}{2}\Big((i_{qs} + i_{qr})i_{dr} - (i_{ds} + i_{dr})i_{qr}\Big), \tag{3.5}$$

where i_{qs}, i_{ds}, i_{qr}, and i_{dr} are the stator and rotor currents, respectively. L_m is the magnetizing inductance of the stator side and T_w can be obtained from the MPPT look-up table for any given wind speed. ω_b is the base frequency, H_t and H_g are the inertia constants of the turbine and the generator, D_t and D_g are the damping coefficients of the turbine and generator, D_{tg} is the damping coefficient of the flexible coupling between the masses, and K_{tg} is the shaft stiffness.

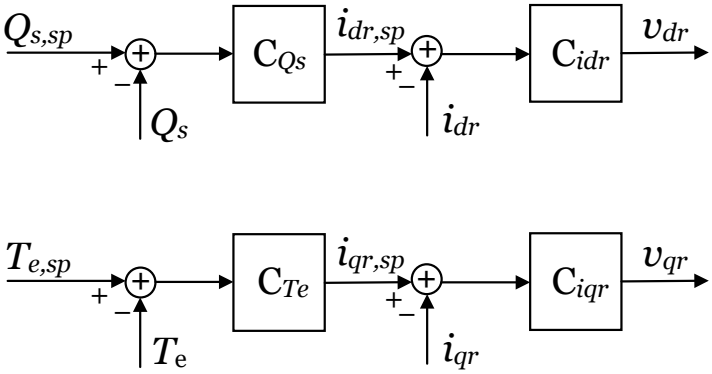

Figure 3.2: Schematic diagram of the RSC controller.

3.3 Induction Generator

The state variables of the induction generator are the stator and rotor currents i_{qs}, i_{ds}, i_{qr}, and i_{dr}. The input variables are the stator and rotor voltages v_{qs}, v_{ds}, v_{qr}, and v_{dr} [22, 23].

$$\frac{d}{dt}\begin{bmatrix} i_{qs} \\ i_{ds} \\ i_{qr} \\ i_{dr} \end{bmatrix} = -\omega_b A_{IG}^{-1} B_{IG} \begin{bmatrix} i_{qs} \\ i_{ds} \\ i_{qr} \\ i_{dr} \end{bmatrix} + \omega_b A_{IG}^{-1} \begin{bmatrix} v_{qs} \\ v_{ds} \\ v_{qr} \\ v_{dr} \end{bmatrix}, \tag{3.6}$$

where

$$A_{IG} = \begin{bmatrix} L_s & 0 & L_m & 0 \\ 0 & L_s & 0 & L_m \\ L_m & 0 & L_r & 0 \\ 0 & L_m & 0 & L_r \end{bmatrix} \tag{3.7}$$

$$B_{IG} = \begin{bmatrix} r_s & \frac{\omega_e L_s}{\omega_b} & 0 & \frac{\omega_e L_m}{\omega_b} \\ -\frac{\omega_e L_s}{\omega_b} & r_s & -\frac{\omega_e L_m}{\omega_b} & 0 \\ 0 & \frac{(\omega_e-\omega_r) L_m}{\omega_b} & r_r & \frac{(\omega_e-\omega_r) L_r}{\omega_b} \\ -\frac{(\omega_e-\omega_r) L_m}{\omega_b} & 0 & -\frac{(\omega_e-\omega_r) L_r}{\omega_b} & r_r \end{bmatrix}. \tag{3.8}$$

In these equations, $L_s = L_{ls} + L_m$ is the sum of stator leakage inductance and magnetizing inductance and $L_r = L_{lr} + L_m$ is the sum of the rotor leakage inductance and magnetizing inductance. ω_e and ω_r are the synchronous frequency and generator rotor speed, respectively, and r_r and r_s are the rotor and stator resistances.

3.4 RSC and GSC Control

The controller of the back-to-back AC/DC/AC converter in a Type III wind generator consists of four control loops that are typically designed using the conventional vector control technique [24]. Figs. 3.2 and 3.3 show the schematic diagram of the RSC and GSC controllers [25]. The rotor-side converter (RSC) injects an AC voltage at slip frequency to the

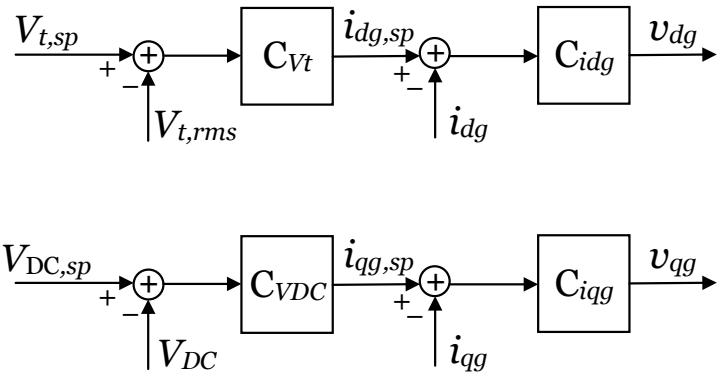

Figure 3.3: Schematic diagram of the GSC controller.

rotor circuit and operates as a controlled voltage source. The GSC injects an AC current at synchronous frequency to the grid and operates as a controlled current source [26]. The GSC and RSC control loops are responsible for maintaining a constant DC link capacitor voltage and controlling the real and reactive power exchange between the turbine and the power grid, respectively [1, 12]. The state equations of the RSC controller are as follows:

$$\frac{di_{dr,sp}}{dt} = \frac{K_{Qs}}{T_{Qs}}(Q_{s,sp} - Q_s) - K_{Qs}\frac{dQ_s}{dt} \tag{3.9}$$

$$\frac{dv_{dr}}{dt} = \frac{K_{idr}}{T_{idr}}(i_{dr,sp} - i_{dr}) + K_{idr}\frac{d(i_{dr,sp} - i_{dr})}{dt} \tag{3.10}$$

$$\frac{di_{qr,sp}}{dt} = \frac{K_{Te}}{T_{Te}}(T_{e,sp} - T_e) - K_{Te}\frac{dT_e}{dt} \tag{3.11}$$

$$\frac{dv_{qr}}{dt} = \frac{K_{iqr}}{T_{iqr}}(i_{qr,sp} - i_{qr}) + K_{iqr}\frac{d(i_{qr,sp} - i_{qr})}{dt} \tag{3.12}$$

The state equations of the GSC controller are as follows:

$$\frac{di_{dg,sp}}{dt} = \frac{K_{Vt}}{T_{Vt}}(V_{t,sp} - V_{t,rms}) - K_{Vt}\frac{dV_{t,rms}}{dt} \tag{3.13}$$

$$\frac{dv_{dg}}{dt} = \frac{K_{idg}}{T_{idg}}(i_{dg,sp} - i_{dg}) + K_{idg}\frac{d(i_{dg,sp} - i_{dg})}{dt} \tag{3.14}$$

$$\frac{di_{qg,sp}}{dt} = \frac{K_{VDC}}{T_{VDC}}(V_{DC,sp} - V_{DC}) - K_{VDC}\frac{dV_{DC}}{dt} \tag{3.15}$$

$$\frac{dv_{qg}}{dt} = \frac{K_{iqg}}{T_{iqg}}(i_{qg,sp} - i_{qg}) + K_{iqg}\frac{d(i_{qg,sp} - i_{qg})}{dt} \tag{3.16}$$

In the RSC control loops, $i_{dr,sp}$, $i_{qr,sp}$, $Q_{s,sp}$, and $T_{e,sp}$ are the set points of qd components of the rotor current, reactive power of the stator, and the electric torque, respectively. In the GSC control loops, $i_{dg,sp}$, $i_{qg,sp}$, $V_{t,sp}$, and $V_{DC,sp}$ are the set points of qd components of the GSC terminal current, terminal bus voltage of turbine, and DC-link voltage, respectively.

3.5 DC-link Capacitor

The dynamic of the DC-link capacitor between the back-to-back converters can be expressed as

$$\frac{dv_{DC}}{dt} = \frac{P_r + P_g}{-Cv_{DC}}, \tag{3.17}$$

where P_r and P_g are the real power of the rotor-side and grid-side converters calculated as

$$P_r = \frac{1}{2}(v_{qr}i_{qr} + v_{dr}i_{dr}) \tag{3.18}$$

$$P_g = \frac{1}{2}(v_{qg}i_{qg} + v_{dg}i_{dg}), \tag{3.19}$$

where v_{qr}, v_{dr}, v_{qg}, and v_{dg} are qd components of the RSC and GSC terminal voltages, respectively [19, 21].

3.6 Series-Compensated Transmission Line

State variables are qd components of the line current (i_{ql}, i_{dl}) and qd components of the voltage across the series capacitor (v_{qc}, v_{dc}).

$$\frac{d}{dt}\begin{bmatrix} i_{ql} \\ i_{dl} \\ v_{qc} \\ v_{dc} \end{bmatrix} = \omega_b A_{TL} \begin{bmatrix} i_{ql} \\ i_{dl} \\ v_{qc} \\ v_{dc} \end{bmatrix} + \omega_b \begin{bmatrix} \frac{(v_{qs}-E_{Bq})}{X_{L,\text{line}}} \\ \frac{v_{ds}-E_{Bd})}{X_{L,\text{line}}} \\ 0 \\ 0 \end{bmatrix}, \tag{3.20}$$

where

$$A_{TL} = \begin{bmatrix} -\frac{R_{\text{line}}}{X_{L,\text{line}}} & -f_e & -\frac{1}{X_{L,\text{line}}} & 0 \\ f_e & -\frac{R_{\text{line}}}{X_{L,\text{line}}} & 0 & -\frac{1}{X_{L,\text{line}}} \\ X_{C,\text{line}} & 0 & 0 & -f_e \\ 0 & X_{C,\text{line}} & f_e & 0 \end{bmatrix}. \tag{3.21}$$

f_e is the rotating frame frequency and E_{Bq} and E_{Bd} are the qd components of the voltage of the infinite bus [5].

4. Proposed Supplementary Controller

4.1 Multiple-Model Adaptive Control Method

The conventional RSC and GSC controllers can handle the normal operation of a Type III wind turbine. However, following a disturbance (e.g., a fault in the system), the power system may tend toward instability. In such cases, an auxiliary controller can be added to the control loop of the wind turbine to prevent the system instability.

In this project, the multiple-model adaptive control (MMAC) approach is used to pro-pose a supplementary controller to operate in a wide range of operating conditions [27, 28]. In MMAC, a finite number of more probable operating conditions are considered and an appropriate linearized dynamic model is derived for each operating point. The main reason for using a linearized model instead of a nonlinear model is that the design and implantation of a linear control technique is more straightforward.

An MMAC controller has two levels; the first level is a set of controllers designed using standard control methods, and the second level is a supervisory controller that selects the level-one controller based on the system conditions [27] (see Fig. 4.1(a)). Although the coefficients of the level-one controllers are fixed, MMAC is called an adaptive approach because it utilizes a large number of model-controller pairs to represent the dynamics of the system.

After a change in the operating point of the system, MMAC uses a vector of feedback signals that have the most impact on the output response of the system to identify the best matching model-controller pair for the current operating condition. Different signals such as the generator rotor speed, real power, and the RMS voltage across the series capacitor are used in the literature as an input control signal [29].

In Fig. 4.1(a), x_1 is the RMS voltage across the series capacitor and vector x_2 is the wind speed and the compensation level. Since f_{el} is related to the wind speed and f_{eo} has a direct relationship with the compensation level, the wind speed and the compensation level are two main parameters that impact the slip s_1 and in turn led to subsynchronous oscillations. For this purpose, a set of more probable and practical wind speeds and compensation levels is considered for use in a look-up table to identify the best matching controller as shown in Fig. 4.1(b). The supervisory controller uses a hysteresis algorithm for the wind speed to switch between the controllers in the look-up table as shown in Fig. 4.1(c).

The controllers in the MMAC bank have a similar structure (a P controller) which are connected to the GSC control loop through a washout filter ($T_w/(1 + sT_w)$), as shown in Fig. 4.2. T_w in this work is equal to 10. These controllers are designed using the root-locus tuning method. While a fixed-parameter controller can operate in a limited operating region, the proposed control technique is shown to provide a significantly better performance for a variable-parameter wind system with a wide operating region [30].

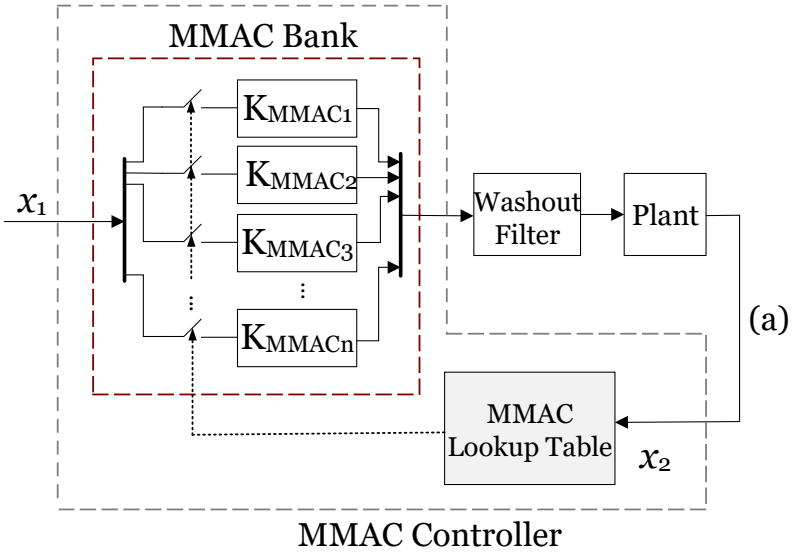

Wind Speed (m/s)	Compensation Level (%)				
	CL≤20	20<CL≤30	30<CL≤40	40<CL≤50	50<CL≤60
$V_w \leq 7$	50	60	70	70	70
$7 < V_w \leq 8$	50	50	70	70	70
$8 < V_w \leq 9$	40	50	60	60	70
$9 < V_w \leq 10$	30	50	50	50	60
$10 < V_w \leq 11$	30	40	50	50	50
$11 < V_w$	20	20	30	40	50

(b)

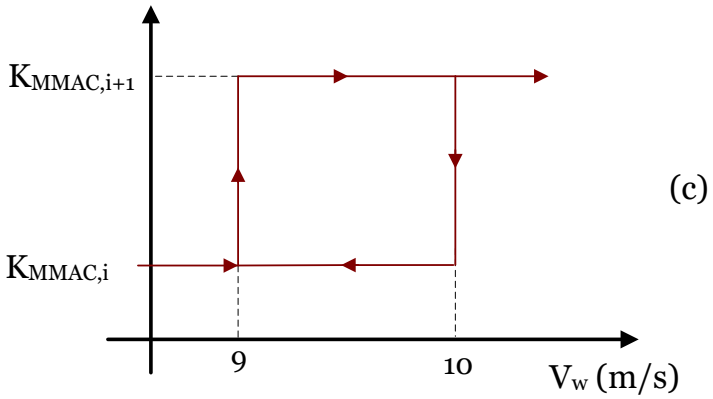

(c)

Figure 4.1: The MMAC approach; (a) block diagram representation of MMAC; (b) example of look-up table.

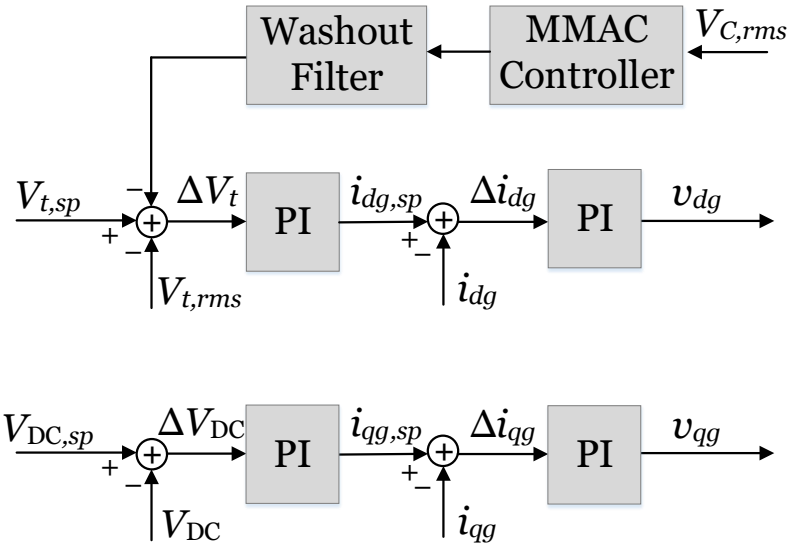

Figure 4.2: Schematic diagram of GSC controller augmented with MMAC strategy.

4.2 Capability of the MMAC Approach in Damping of SSR

In this subsection, the impact of the MMAC-based supplementary controller in damping of SSR is studied. The input control signal of MMAC is the RMS voltage across the series capacitor ($V_{C,rms}$). As the compensation level increases the voltage across the series capacitor increases ($V_{C,rms} \propto X_C$). Moreover, in GSC control loop, ΔV_t can be calculated as

$$\Delta V_t = V_{t,sp} - V_{t,rms} - K_{\text{MMAC}} V_{C,rms}, \tag{4.1}$$

where K_{MMAC} is the gain of MMAC. As depicted in Fig. 4.2, the GSC terminal voltage injection (V_{dg} and V_{qg}) has a direct relationship with the GSC terminal current injection (Δi_{dg} and Δi_{qg}) and this is equivalent to a resistance in the stator circuit. The relationship between the stator voltage and current (V_s and I_s) and the GSC terminal voltage and current (V_g and I_g) can be expressed as

$$V_s = V_g - \mathrm{j} X_{tg} I_g \tag{4.2}$$

$$I_s = I_g + I_{\text{Line}}, \tag{4.3}$$

where X_{tg} is the grid-side transformer reactance and I_{Line} is the transmission line current. Therefore, MMAC has a direct impact on V_s and I_s and as a result on the damping of SSR ($|r_{r,\text{eq}}| > |R_{\text{line}} + V_s/I_s|$). A higher stator resistance can improve the positive damping of SSR.

4.3 Stability Analysis of the MMAC Approach

Switching between stable subsystems will not necessarily result in a globally stable system [31]. However, the main condition for having a globally stable system is that all the

submodels and corresponding controllers must be globally stable. Moreover, switching between submodels needs to be controlled to guarantee a globally stable process. In [32], it is shown that, "the overall system will be globally stable for any arbitrary switching sequence, provided that the intervals between successive switches have a nonzero lower bound $T_{\min} > 0$, which can be chosen to be arbitrarily small." The supervisory controller in the proposed control technique uses a hysteresis algorithm which avoids the uninterrupted switching $(T_{i+1} - T_i = 0)$ between the controllers in the look-up table. Therefore, the mentioned restriction is feasible in this application [33]. In this work, all the subsystems have identical structures; therefore, the global stability of one model with the proposed controller results in the global stability of all the subsystems.

4.4 Coordination of the Supplementary Controllers in a Nonaggregated Wind System

In this section, a systematic approach is introduced for simultaneous coordination of parameters of the supplementary controllers in a nonaggregated wind system. In this method, the linearized model of the system is used to develop a relationship between the parameters of the supplementary controllers and the eigenvalues of the system. Fig. 4.3 summarizes the proposed algorithm.

4.4.1 Relationship Between the Parameters of the Controllers and Eigenvalues of the System

The dynamic of a system can be expressed by a set of n first-order nonlinear ordinary differential equations as follows

$$\dot{x} = f(x, u), \tag{4.4}$$

where $x = [x_1, x_2, ..., x_n]^T$ is the state vector and $x_1, x_2, ..., x_n$ are state variables of system. $u = [u_1, u_2, ..., u_r]^T$ is the input vector of the dynamic system. The output variables of system also can be expressed as a vector of non-linear functions as follows

$$y = g(x, u), \tag{4.5}$$

where $y = [y_1, y_2, ..., y_m]^T$ is the output vector and $g(x, u)$ is a vector consists of non-linear functions that relates the output variables to the state and input variables of the dynamic system. The eigenvalue sensitivity analysis is a tool to find a relationship between the parameters of the interest and the eigenvalues of the system. For this purpose, the parametric state-space of the system can be developed using a mathematical software tool.

$$\Delta\dot{x} = A\Delta x + B\Delta u \tag{4.6}$$

$$\Delta y = C\Delta x + D\Delta u, \tag{4.7}$$

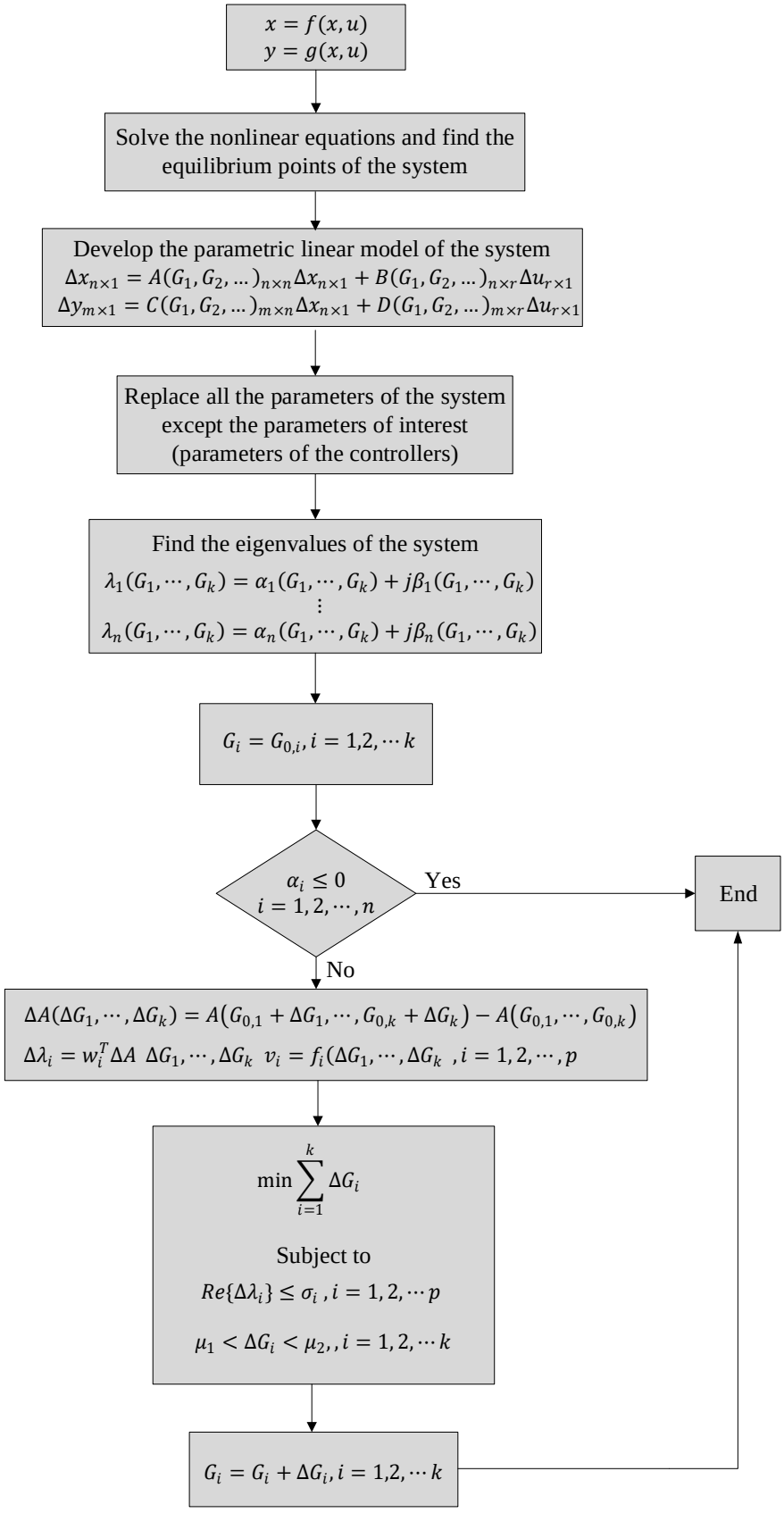

Figure 4.3: Flow chart of the proposed method.

where A, B, C, and D are the parametric state, input, output, and feed-forward matrices, respectively, and can be calculated as

$$A = \frac{\partial f(x,u)}{\partial x} \tag{4.8}$$

$$B = \frac{\partial f(x,u)}{\partial u} \tag{4.9}$$

$$C = \frac{\partial g(x,u)}{\partial x} \tag{4.10}$$

$$D = \frac{\partial g(x,u)}{\partial u}. \tag{4.11}$$

By replacing all the parameters of the system with their given values except the parameters of the controllers $(G_1, G_2, ..., G_k)$ elements of A can be represented as nonlinear functions of $G_1, G_2, ..., G_k$. To find the critical modes of the system, a set of initial values can be chosen for the parameters of the controller and the eigenvalues of the system can be calculated.

$$\lambda_i(G_{0,1}, \ldots, G_{0,n}) = \alpha_i(G_{0,1}, \ldots, G_{0,n}) + j\beta_i(G_{0,1}, \ldots, G_{0,n}), i = 1, \ldots, n, \tag{4.12}$$

where α_i and β_i are the real and imaginary parts of the eigenvalues and n is number of eigenvalues of the system. At this point, the critical eigenvalues corresponding to unstable modes of the system can be identified.

Based on [34], the sensitivity of a eigenvalue λ_i of matrix A respect to a parameter G can be calculated as

$$\frac{\partial \lambda_i}{\partial G} = w_i^T \frac{\partial A}{\partial G} v_i, \tag{4.13}$$

where w_i and v_i are the normalized left and right eigenvectors corresponding to λ_i (the critical mode of system), respectively. Using (4.13), an equation can be developed to find the sensitivity of λ_i to a small change in an element of matrix A.

$$\Delta\lambda_i = w_i^T \Delta A(\Delta G_1, \ldots, \Delta G_k) v_i, i = 1, \ldots, p \tag{4.14}$$

$$\Delta A(\Delta G_1, \ldots, \Delta G_k) = A(G_{0,1} + \Delta G_1, \ldots, G_{0,k} + \Delta G_k) - A(G_{0,1}, \ldots, G_{0,k}), \tag{4.15}$$

In practice, a system can have two or more poorly-damped or unstable eigenvalues. In (4.14), p is the number of eigenvalues of the system in the right–hand side. Using (4.14), a linear equation based on the parameters of the controllers can be developed for each unstable eigenvalues.

4.4.2 Coordination of the Parameters of the Supplementary Controller

In previous subsection, a series of equations are developed for poorly-damped or unstable modes of the system to predict the left shift of the eigenvalues based on the change in the parameters of the controllers. In this subsection, an optimization approach is used to simultaneously find the gains of the controllers. The aims of the coordination approach are

to (1) stabilize system by moving the unstable modes to the left–hand side, (2) improve the damping ratio of the poorly-damped modes, and (3) minimize the controllers gain values. For this purpose, using (4.14) a linear programming problem can be developed as follows

$$\begin{aligned} \text{minimize} \quad & \sum_{i=1}^{k} \Delta G_i \\ \text{subject to} \quad & Re\{\Delta\lambda_i\} \leq \sigma_i, i = 1, 2, \ldots, p \\ & \mu_1 < \Delta G_i < \mu_2, i = 1, 2, \ldots, k \end{aligned} \tag{4.16}$$

where σ_i is the desired left shift for the eigenvalue i, and μ_1 and μ_2 are the lower and upper bands for the gain increments. This minimization problem can be solved using the wellknown optimization algorithms [35]. The optimal values of parameters of the controllers can be calculated as

$$G_i = G_{0,i} + \Delta G_i, i = 1, 2, \ldots, k. \tag{4.17}$$

5. Performance Evaluation

5.1 Aggregated System

This section presents case studies to evaluate the performance of the proposed control technique. Small-signal stability analysis of the system is performed in MATLAB. Transient analysis of the system is conducted in PSCAD/EMTDC software.

The study system is an aggregated 5 MW Type III-based wind farm connected to a 33 kV series-compensated line (R_L is 1.452 Ω, X_L is 22.808 Ω, and X_c is 11.404 Ω at 50% compensation level) shown in Fig. 5.1. The nominal voltage of the wind farm terminal bus is 690 V. The rated power of the wind farm is 5 MVA and the base frequency is 50 Hz.

5.1.1 Small-Signal Stability Analysis

In this subsection, the small-signal stability of the study system for different operating conditions and with and without the supplementary MMAC controller is studied. In all the case studies, it is assumed that because of a fault, before $t = 0\,\text{s}$ the wind turbine is radially connected to the compensated transmission line.

The base system

The eigenvalue analysis of the base system (without the supplementary MMAC controller intervention) at a wind speed of 8 m/s and a compensation level of 60% is studied. Table 5.1 shows the eigenvalues of the system and their corresponding damping ratios. At a wind speed of 8 m/s and compensation level of 60%, there is an unstable mode in the system with −2.25% negative damping and frequency of 27.58 Hz (subsynchronous mode). Eigenvalue analysis verifies the point that, under some operating conditions, the subsynchronous interaction is

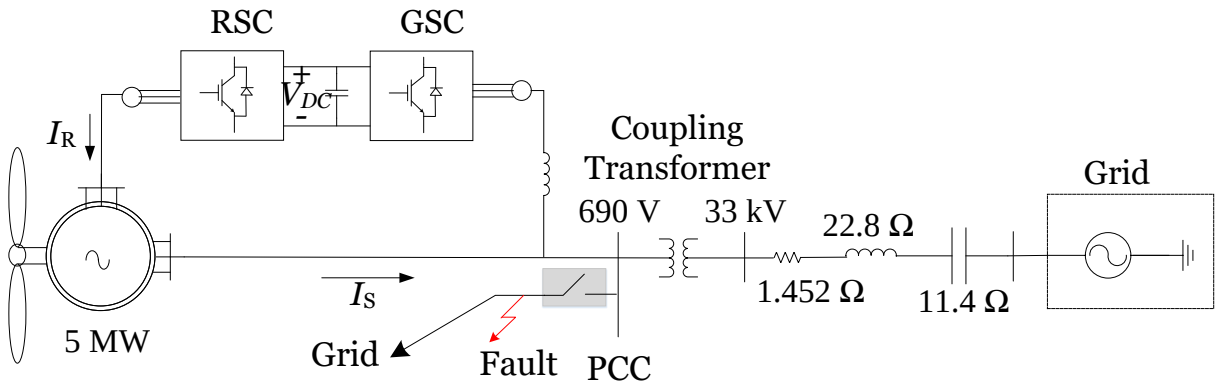

Figure 5.1: Schematic diagram of the studied aggregated system.

TABLE 5.1
EIGENVALUES OF THE SYSTEM AT A WIND SPEED OF 8 M/S AND A COMPENSATION LEVEL OF 60%.

Eigenvalue (rad/s)	**Damping ratio (%)**
−4885	-
−1990 ± j3399	50.53
−9.71 ± j452.64	2.14
3.91 ± j173.34	**−2.25**
−17.05 ± j139.48	12.13
−10.00	-
−9.21	-
−1.29 ± j8.93	14.36
−0.50	-
−0.02 ± j0.25	7.97
−0.01	-
−0.02	-
−0.00	-
−0.00	-

likely in a series-compensated wind system and emphasizes the need for a strategy to improve the transient response of the system.

Change in the compensation level

This case study analyzes the small signal stability of the system under different operating conditions without the supplementary controller. For this purpose, the eigenvalues of the system for three different wind speeds (7 m/s, 8 m/s, and 10 m/s) with varying compensation levels are shown in Figs. 5.2–5.4. In these figures, the arrows show the movement of the eigenvalues of the system as the compensation level increases from 30% to 80%.

Fig. 5.2 shows the eigenvalues of the system for a wind speed of 7 m/s under different compensation levels. As the compensation level increases from 30% to 80%, some eigenvalues move from the left-hand side to the right-hand side and the system becomes unstable. Similarly, as shown in Fig. 5.3, with a constant wind speed of 8 m/s, as the compensation level increases from 30% to 80%, some eigenvalues move from the left-hand side to the right-hand side. However, system is more stable at 8 m/s. When the wind speed increases to 10 m/s (see Fig. 5.4), system remains stable when the compensation level increases from 30% to 80%.

Eigenvalue analysis with supplementary controller

This case study shows the performance of the proposed supplementary controller. Figs. 5.5 and 5.6 show the eigenvalues of the system at a wind speed of 7 m/s and under different compensation levels with and without the supplementary controller. In Figs. 5.5 and 5.6, the arrows show the movement of the eigenvalues of the system when the proposed supplementary controller is added to the system.

It can be seen that without the supplementary controller, there is an unstable mode in the system at 33.42 Hz (subsynchronous mode). However, the eigenvalues move toward the

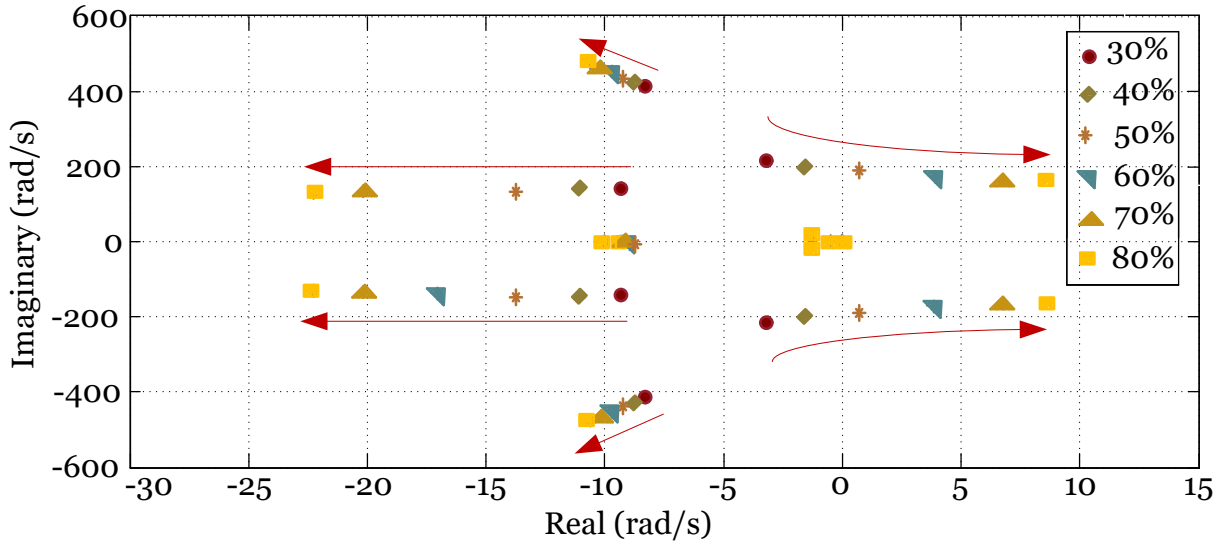

Figure 5.2: Eigenvalues of the system at a wind speed of 7 m/s under different compensation levels.

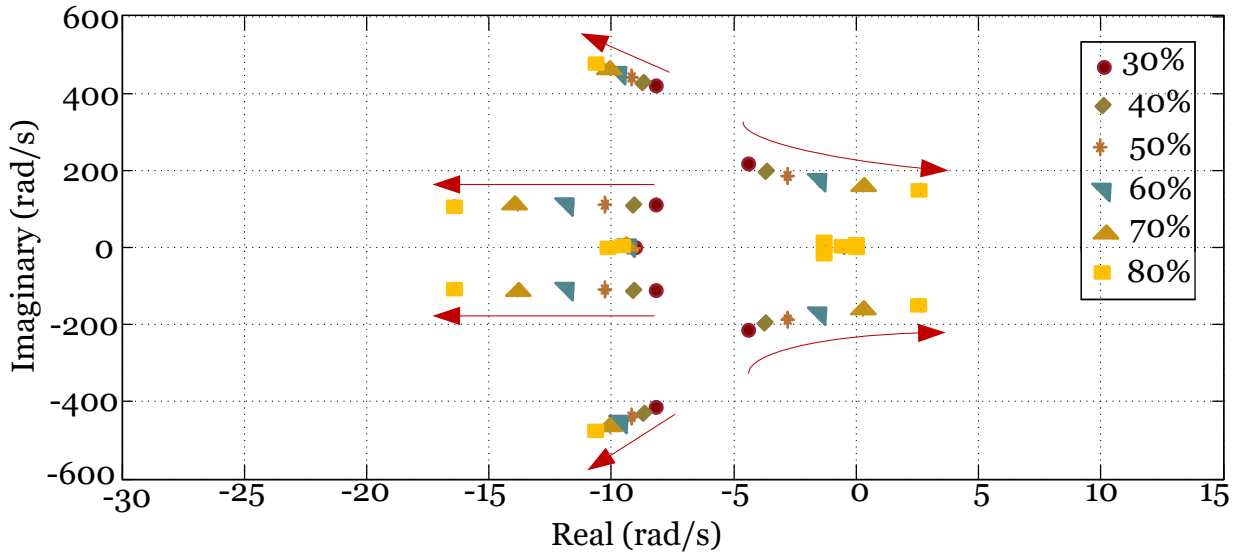

Figure 5.3: Eigenvalues of the system at a wind speed of 8 m/s under different compensation levels.

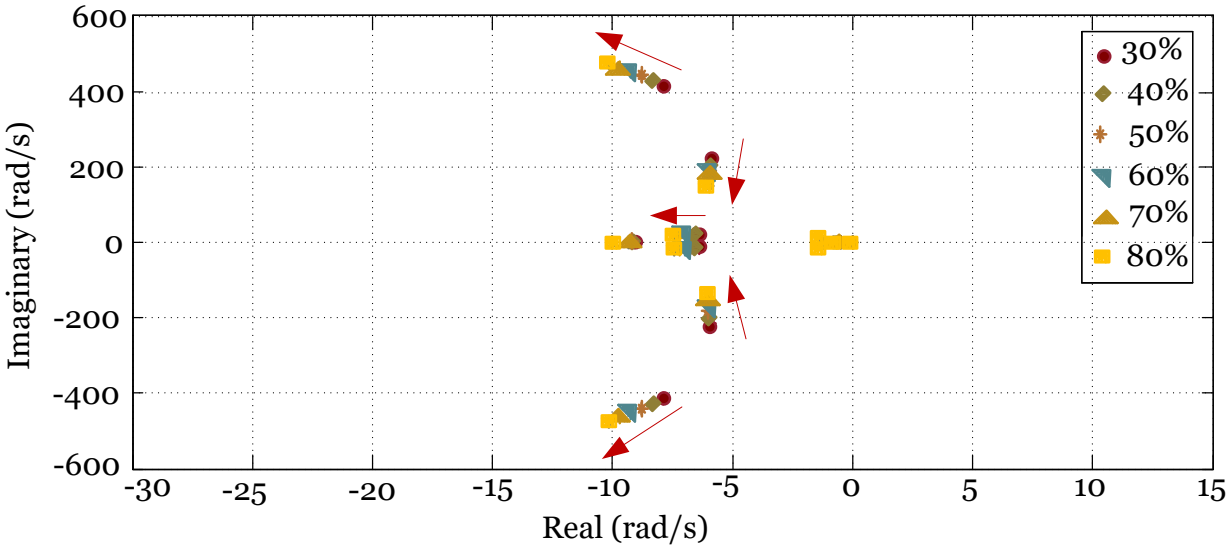

Figure 5.4: Eigenvalues of the system at a wind speed of 10 m/s under different compensation levels.

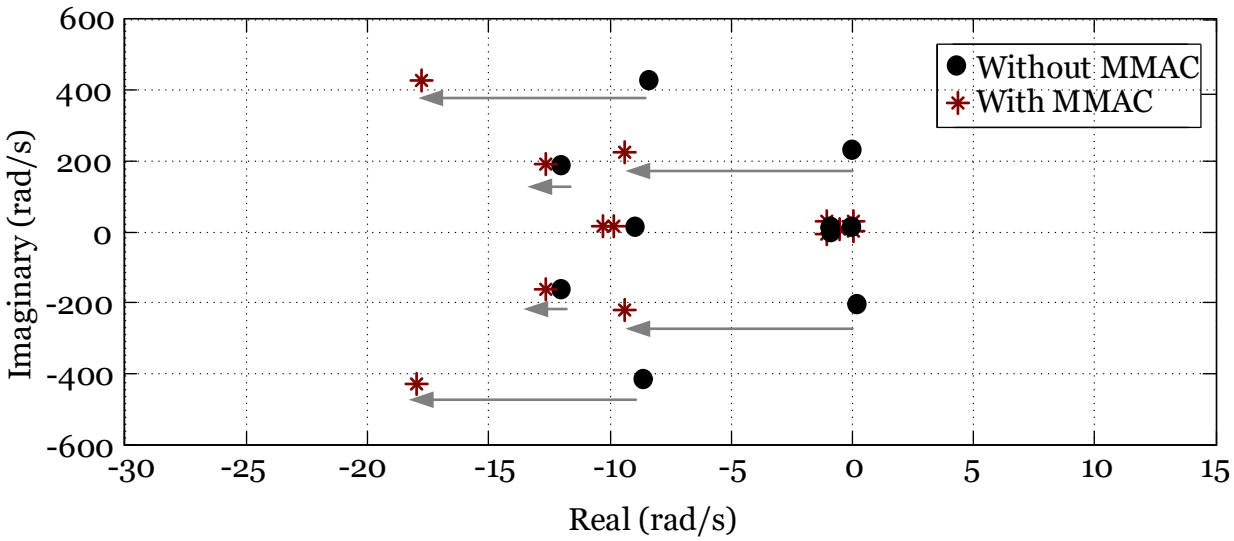

Figure 5.5: Eigenvalues of the system at a wind speed of 7 m/s and 30% compensation level with and without the supplementary controller.

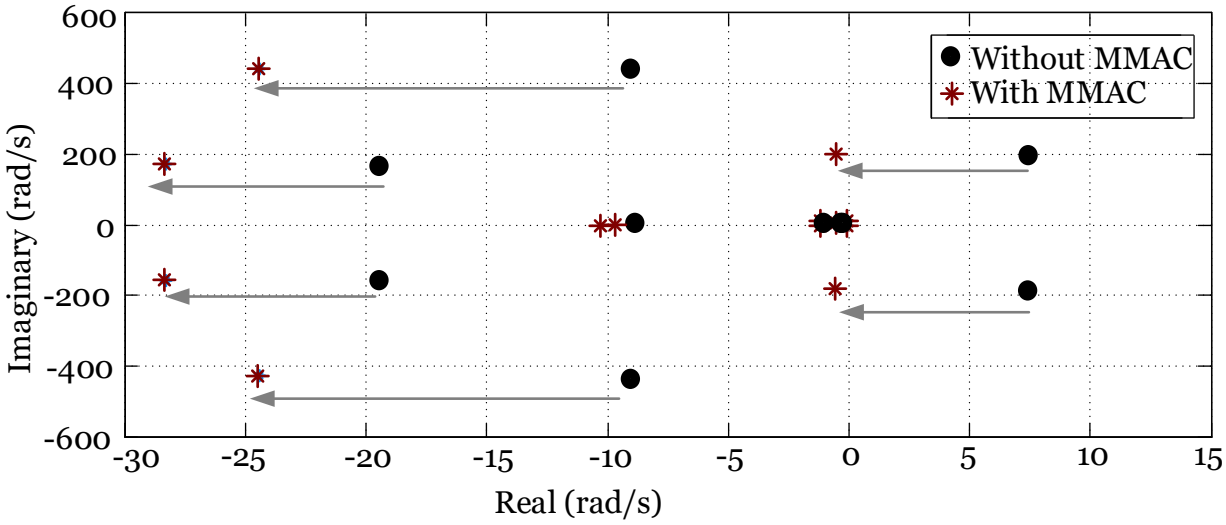

Figure 5.6: Eigenvalues of the system at a wind speed of 7 m/s and 50% compensation level with and without the supplementary controller.

left-hand side and the system becomes stable when the supplementary controller is added to the control loop of the wind turbine.

5.1.2 Transient Stability Analysis

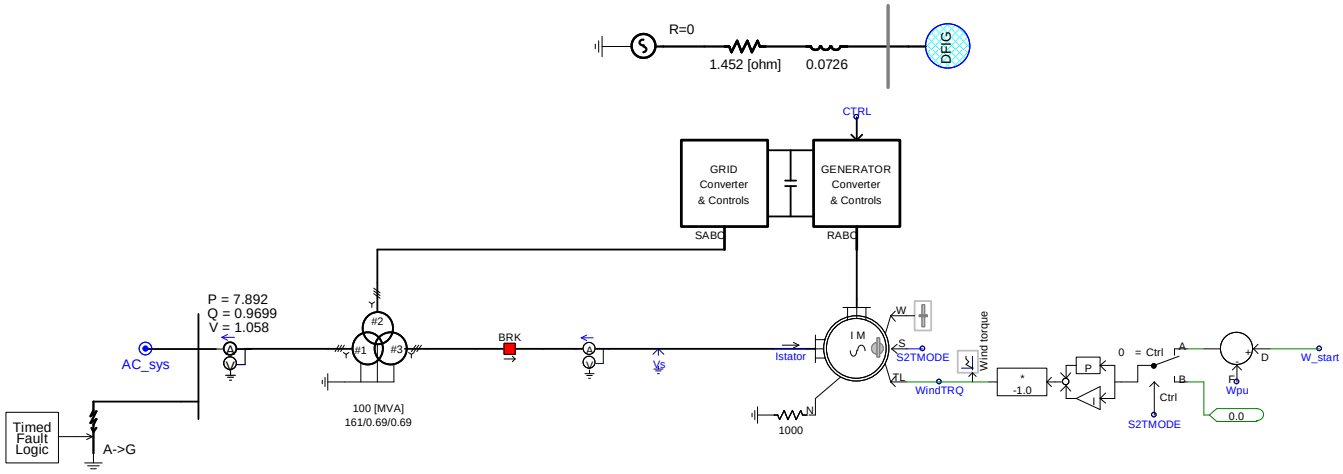

Figure 5.7: Study system model in PSCAD/EMTDC.

In this subsection, the transient stability of the study system for different operating conditions with and without the supplementary controller intervention is studied. Fig. 5.7 shows the system model in PSCAD/EMTDC software.

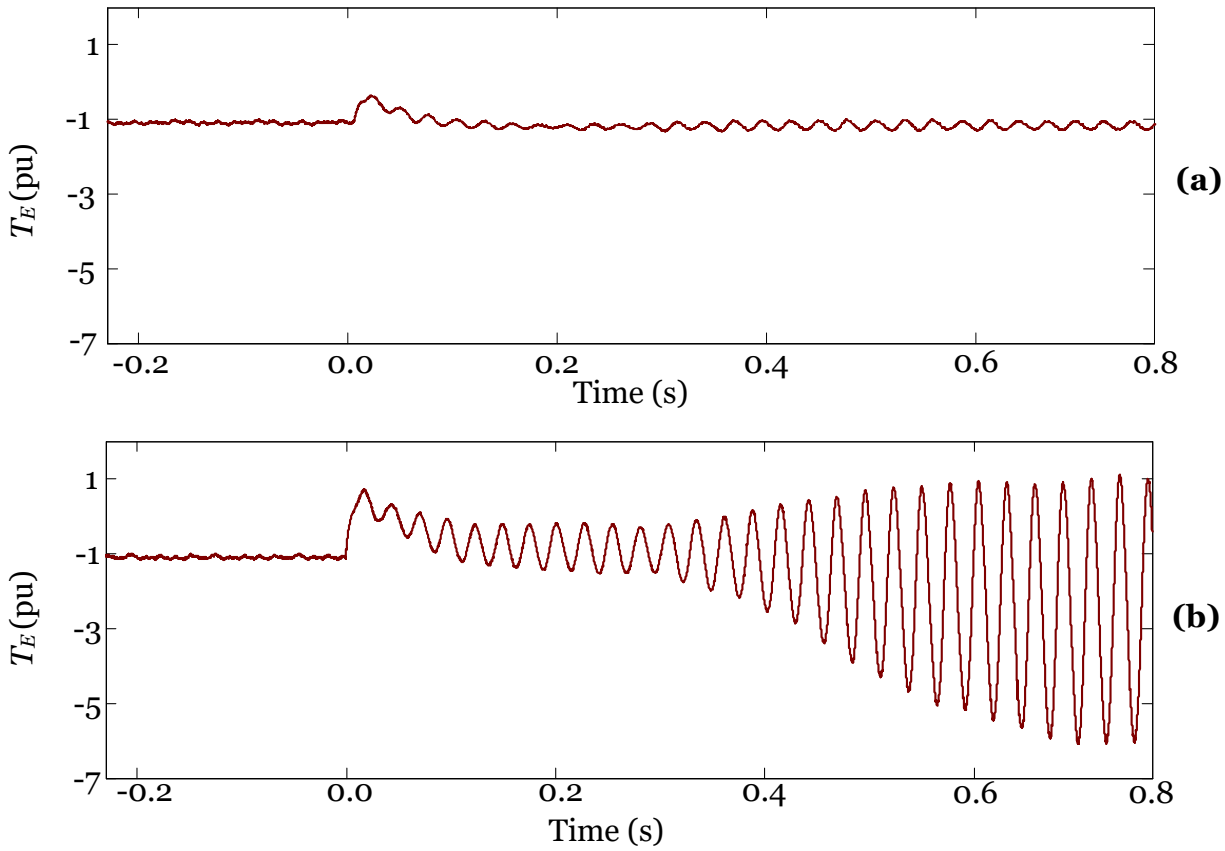

Figure 5.8: Response of electric torque of DFIG to a step change in the wind speed at $t = 0\,\text{s}$; (a) from 12 m/s to 10 m/s; (b) from 12 m/s to 8 m/s.

Step change in the wind speed for the base system

This case study evaluates the performance of the conventional controllers of the wind turbine for a step change in the wind speed at time $t = 0\,\text{s}$. The compensation level for this case study is 50%.

Fig. 5.8(a) shows the response of the electric torque of DFIG to a change in the wind speed from 12 m/s to 10 m/s at $t = 0\,\text{s}$. In this case, after the step change in the wind speed the system still remains stable. It shows that the conventional controllers of the RSC and GSC can handle the operation of the wind turbine in some operating conditions.

Fig. 5.8(b) shows the response of the electric torque of DFIG to a change in the wind speed from 12 m/s to 8 m/s at $t = 0\,\text{s}$. Before the step change in the generator rotor speed system is stable. However, after the step change, the system becomes unstable and this emphasizes the need for a supplementary controller. In general, eigenvalues of the system move toward the left-hand side when the wind speed increases and the compensation level decreases and the system becomes stable.

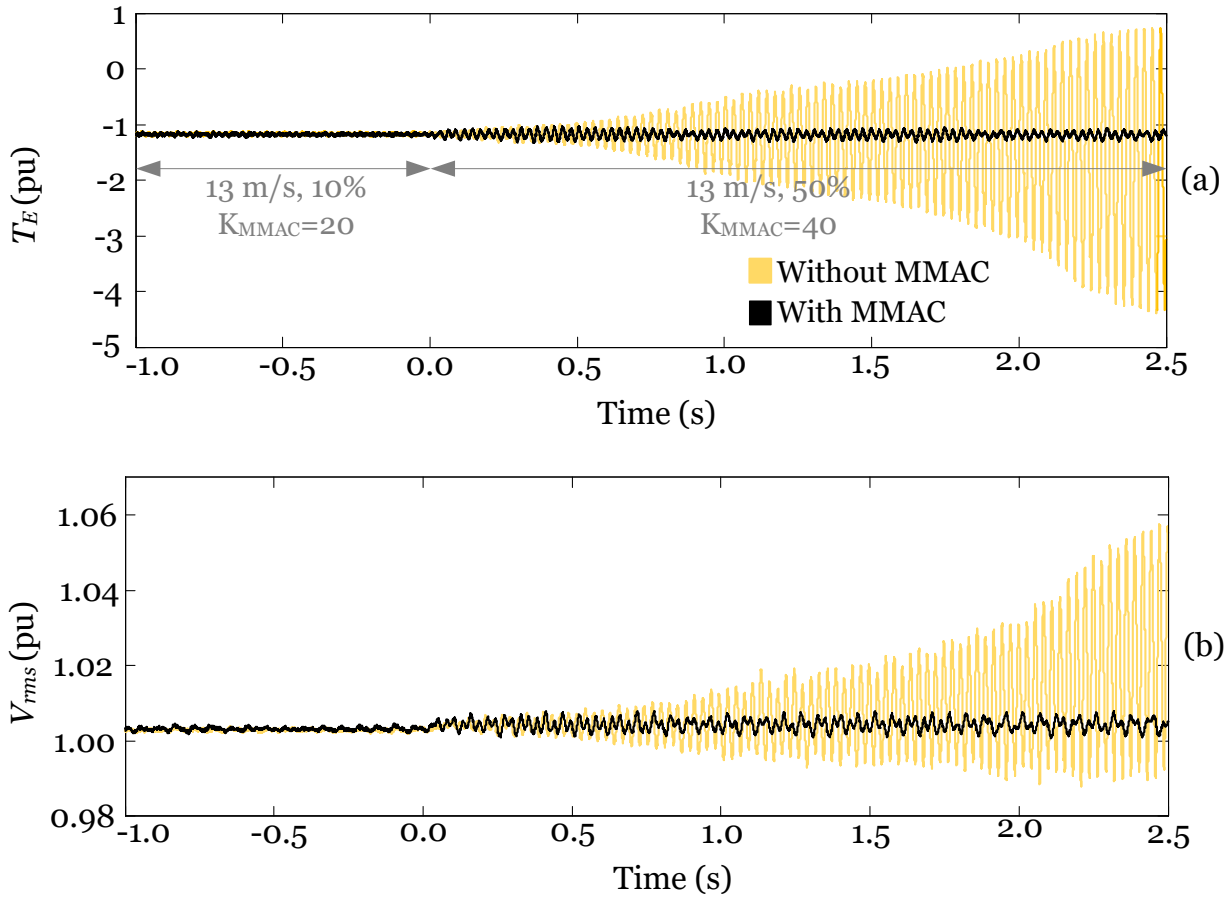

Figure 5.9: Response to a step change in the compensation level from 10% to 50% at $t = 0\,\text{s}$; (a) electric torque of DFIG; (b) RMS voltage of PCC.

Step change in the compensation level

In this case study, the response of the system to a step change in the compensation level from 10% to 50% at time $t = 0\,\text{s}$ is studied. The wind speed for this case study is 13 m/s. Figs. 5.9(a) and (b) show the response of the electric torque of DFIG and the RMS voltage of PCC with and without the supplementary controller.

Fig. 5.9(a) shows the response of the electric torque of DFIG with and without the supplementary controller. The response of the system without the supplementary controller becomes unstable after $t = 0\,\text{s}$. However, the response of the electric torque of DFIG with the supplementary controller remains stable. Similarly, in Fig. 5.9(b), as the compensation level increases from 10% to 50%, system becomes unstable. However, when the supplementary controller is added to the system, the response of the system remains stable.

Step change in the wind speed

In this case study, the response of the system to a step change in the wind speed from 10 m/s to 7 m/s at time $t = 0\,\text{s}$ is studied. The compensation level for this case study is 50%. Figs. 5.10(a) and (b) show the response of the electric torque of DFIG and the RMS

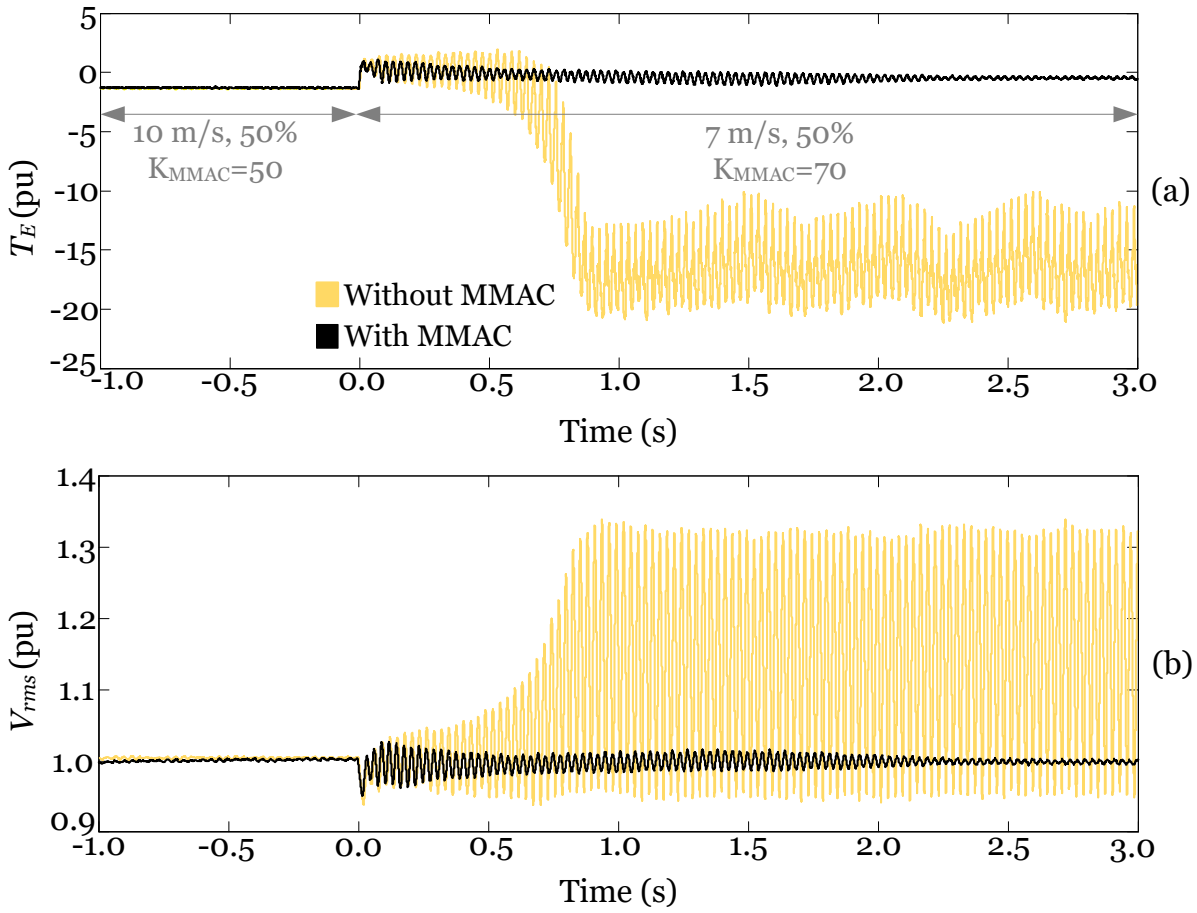

Figure 5.10: Response to a step change in the wind speed from 10 m/s to 7 m/s at $t = 0\,\text{s}$; (a) electric torque of DFIG; (b) RMS voltage of PCC.

voltage of PCC with and without the supplementary controller.

Fig. 5.10(a) shows the response of the electric torque of DFIG with and without the supplementary controller. The response of the system without the supplementary controller becomes unstable after $t = 0\,\text{s}$. However, the response of the electric torque of DFIG with the supplementary controller remains stable. Similarly, in Fig. 5.10(b), as the wind speed decreases from 10 m/s to 7 m/s, system becomes unstable. However, when the supplementary controller is added to the system, the response of the system remains stable.

Three-phase to ground fault

In this case study, the response of the system to a three-phase to ground fault that occur at PCC at time $t = 0\,\text{s}$ and clears after $0.25\,\text{s}$ is studied. The wind speed is 6 m/s. Figs. 5.11(a) and (b) show the response of the electric torque of DFIG and the RMS voltage of PCC with and without the supplementary controller.

In this case study, following a topology change in the system due to the fault in PCC, the wind turbine is radially connected to a 40% series-compensated line. During the normal operation of the system (before the fault and after it is cleared), the equivalent compensation

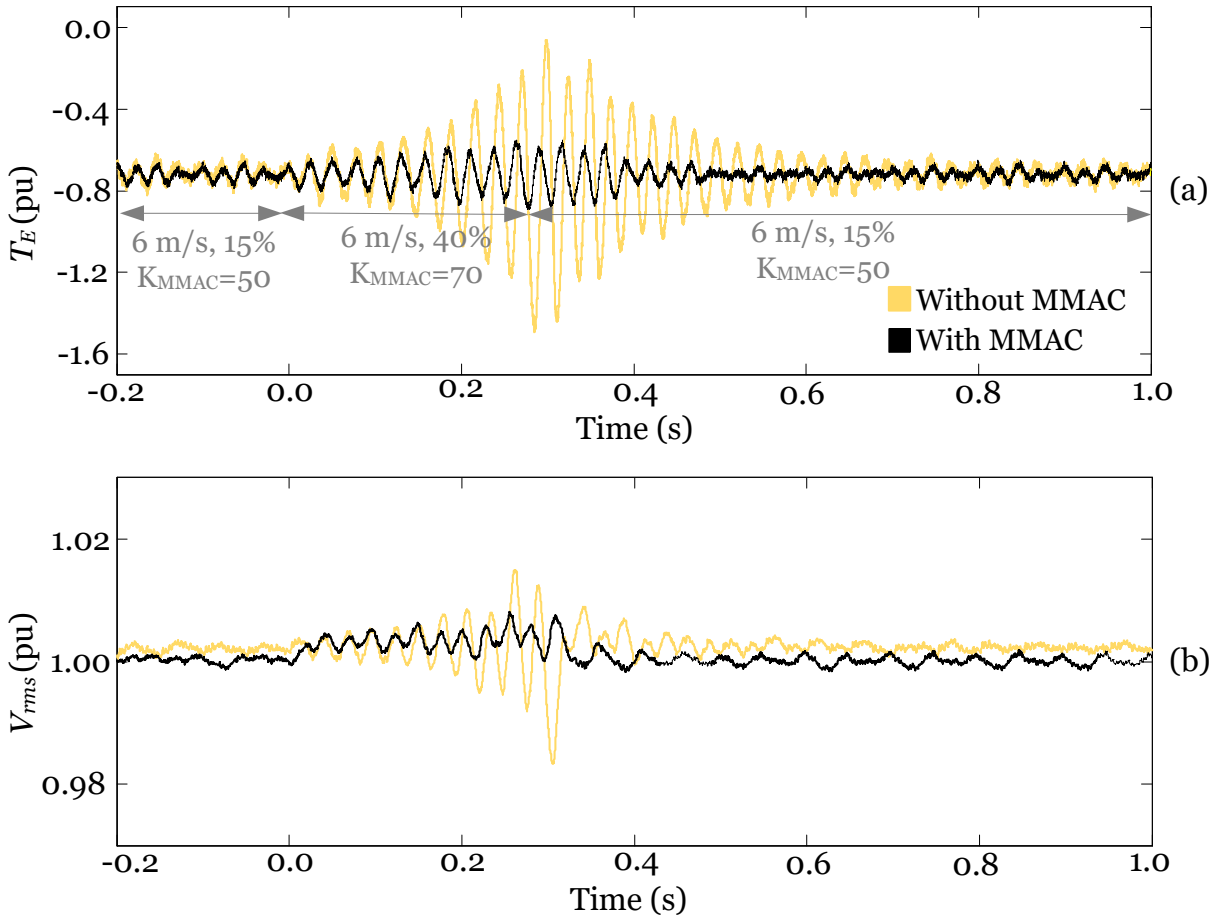

Figure 5.11: Response to a three-phase to ground fault at time $t = 0\,\text{s}$ and cleared after $0.25\,\text{s}$; (a) electric torque of DFIG; (b) RMS voltage of PCC.

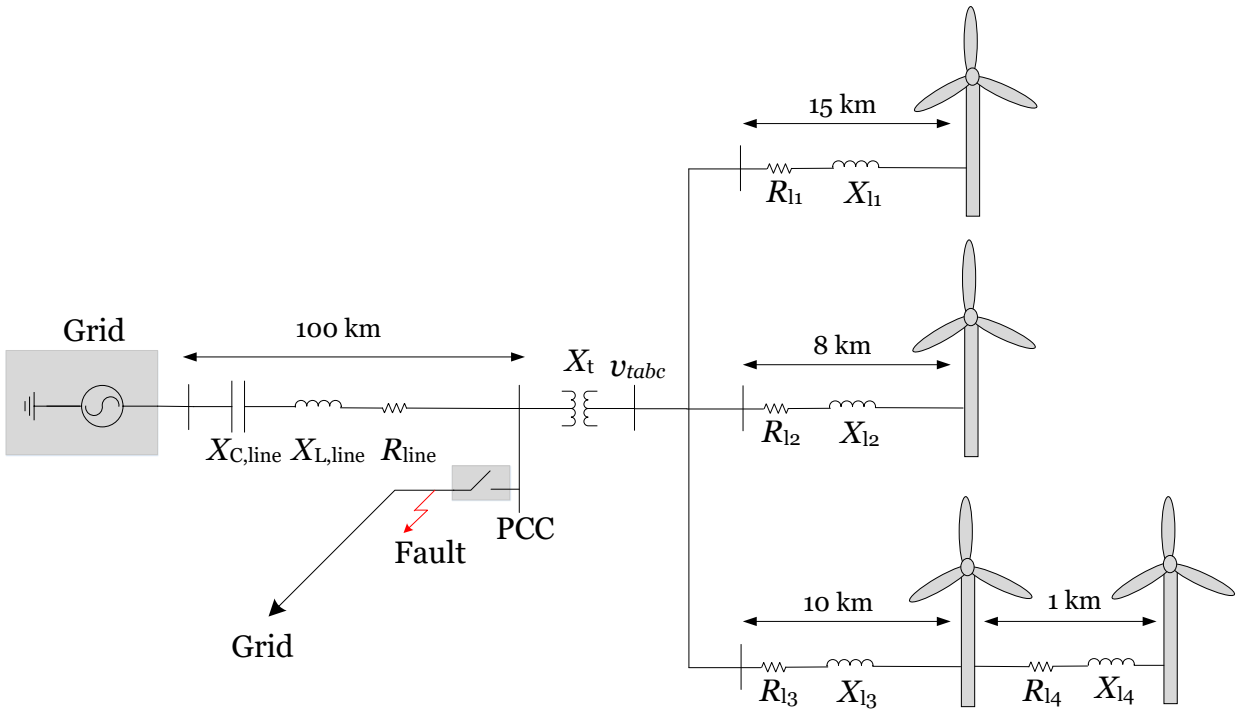

Figure 5.12: Schematic diagram of the studied nonaggregated system.

level is assumed to be 15%. Fig. 5.11(a) shows the response of the electric torque of DFIG with and without the supplementary controller. The maximum and minimum peak values of the response without the supplementary controller are -0.15 pu and -1.55 pu, respectively, and response settles after 40 m/s. However, when the supplementary controller is active, the maximum peak value reduces to -0.65 pu and the minimum peak value increases to -0.90 pu, respectively. This improvement leads to a settling time of about 20 m/s. The response of the RMS voltage of PCC with and without the supplementary controller is shown in Fig. 5.11(b). The results show the superior performance of the MMAC-based supplementary controller for damping of SSR compared to the case without the supplementary controller.

5.2 Nonaggregated System

In this section, a nonaggregated 20 MW Type III wind farm consists of 3 feeders with a varying number of connected wind turbines and a varying distance from PCC is developed. The wind farm is connected to a 33 kV series compensated line (R_{line} is 3.7 Ω, $X_{\text{L,line}}$ is 36.7 Ω, X_t is 13.06 Ω, and $X_{\text{C,line}}$ is 25.5 Ω at 50% compensation level) shown in Fig. 5.12. The nominal voltage of the wind farm terminal bus is 690 V and the nominal voltage of the network is 33 kV. The rated power of each wind turbine is 5 MVA.

The base system

This case study evaluates the stability of the study system to the changes in the wind speed and the compensation level at different time instances. Figs. 5.13–5.16(a) and (b) show the

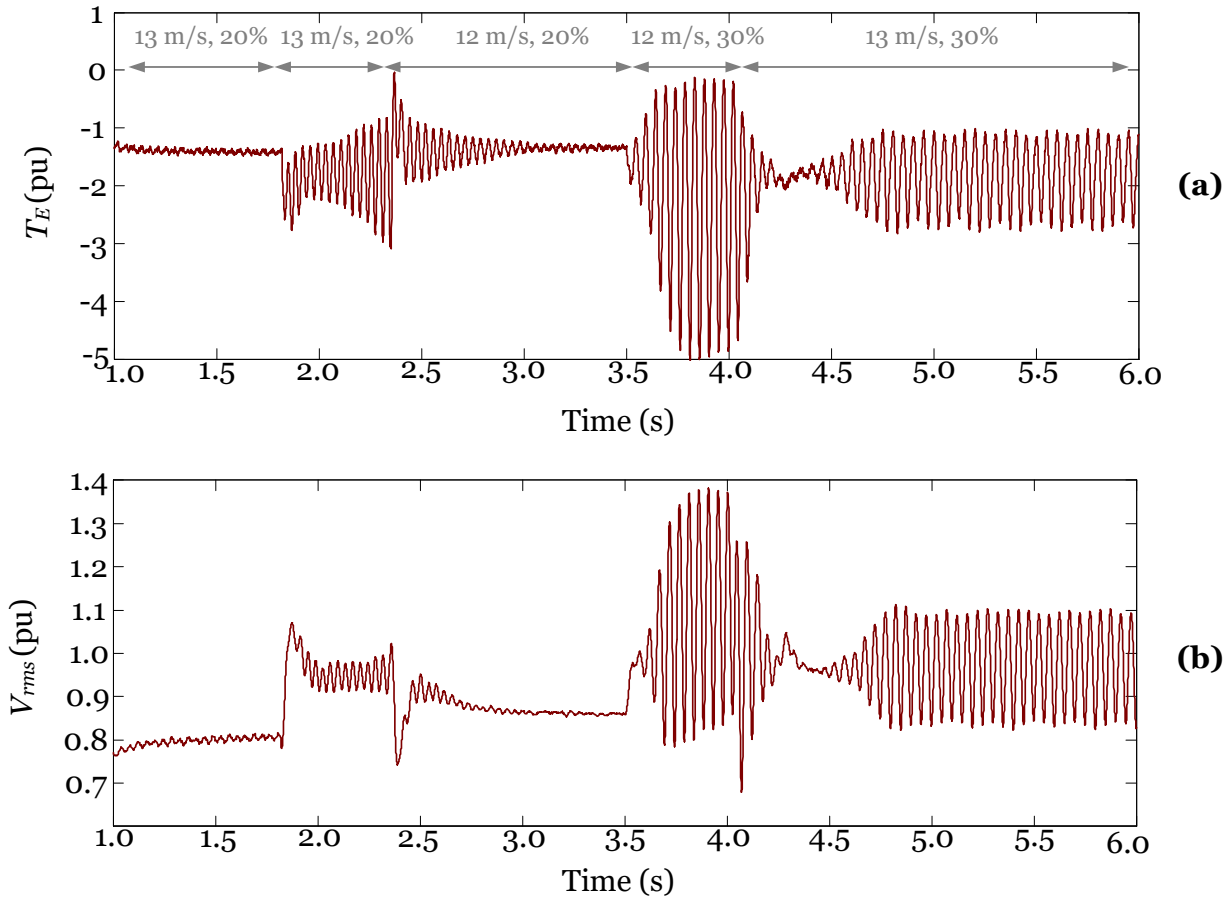

Figure 5.13: Response of the wind turbine 1 to the changes in the wind speed and the compensation level; (a) electric torque of DFIG; (b) RMS voltage of PCC.

response of the electric torque of the DFIG and RMS voltage of the PCC to the changes in the wind speed and the compensation level in the wind turbines 1, 2, 3, and 4, respectively. The compensation level and the wind speed are varying during the simulation time.

It can be seen that wind turbines show a similar behavior to the changes that occur in the wind speed and compensation level. For instance, at $t = 1.8\,\text{s}$ the wind speeds of wind turbines 2, 3, and 4 change from 13 m/s to 8 m/s, 10 m/s, and 10 m/s, respectively and the wind speed of turbine 1 remains constant. However, all the wind turbines become unstable after $t = 1.8\,\text{s}$. This case study emphasizes the need for a coordination algorithm for the supplementary controllers of the wind turbines in a wind farm.

5.2.1 Step Change in the Compensation Level

This case study evaluates the stability of the study system for the changes in the compensation level at different time instances. Figs. 5.17–5.19(a) and (b) show the response of the electric torque of wind turbines 1–4 to a step change in the compensation level from 30% to 50% at time $t = 2\,\text{s}$ with and without the MMAC-based supplementary controller. The compensation level is returned to 30% at $t = 3\,\text{s}$.

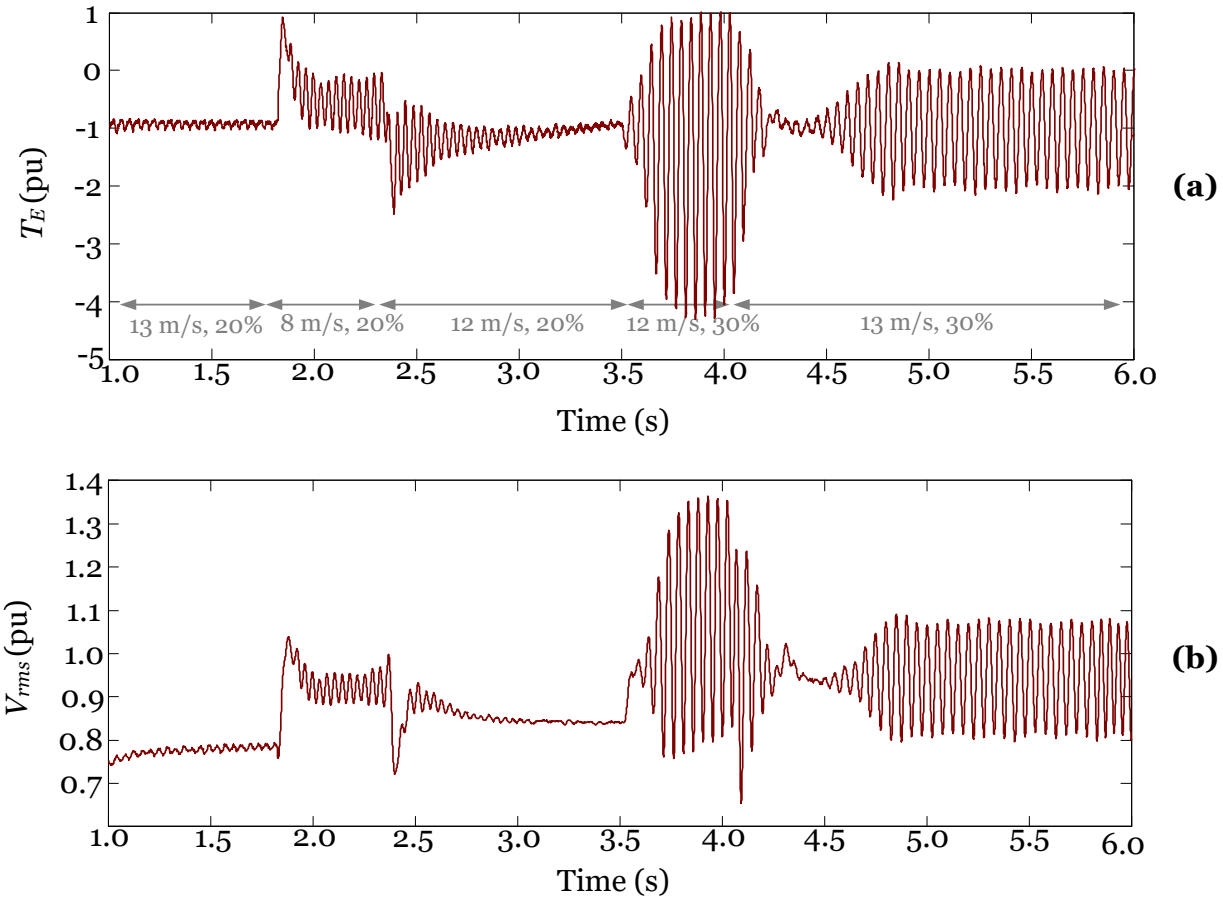

Figure 5.14: Response of the wind turbine 2 to the changes in the wind speed and the compensation level; (a) electric torque of DFIG; (b) RMS voltage of PCC.

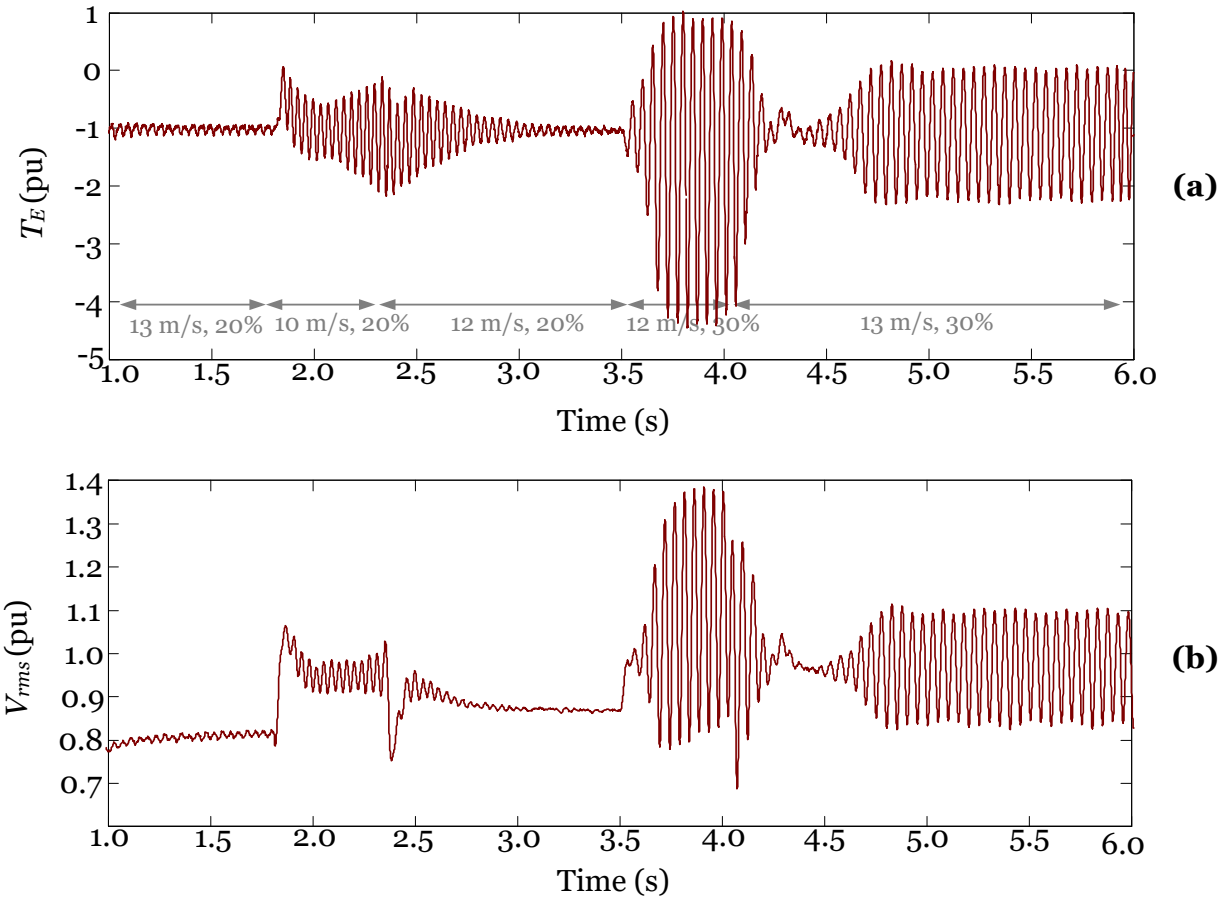

Figure 5.15: Response of the wind turbine 3 to the changes in the wind speed and the compensation level; (a) electric torque of DFIG; (b) RMS voltage of PCC.

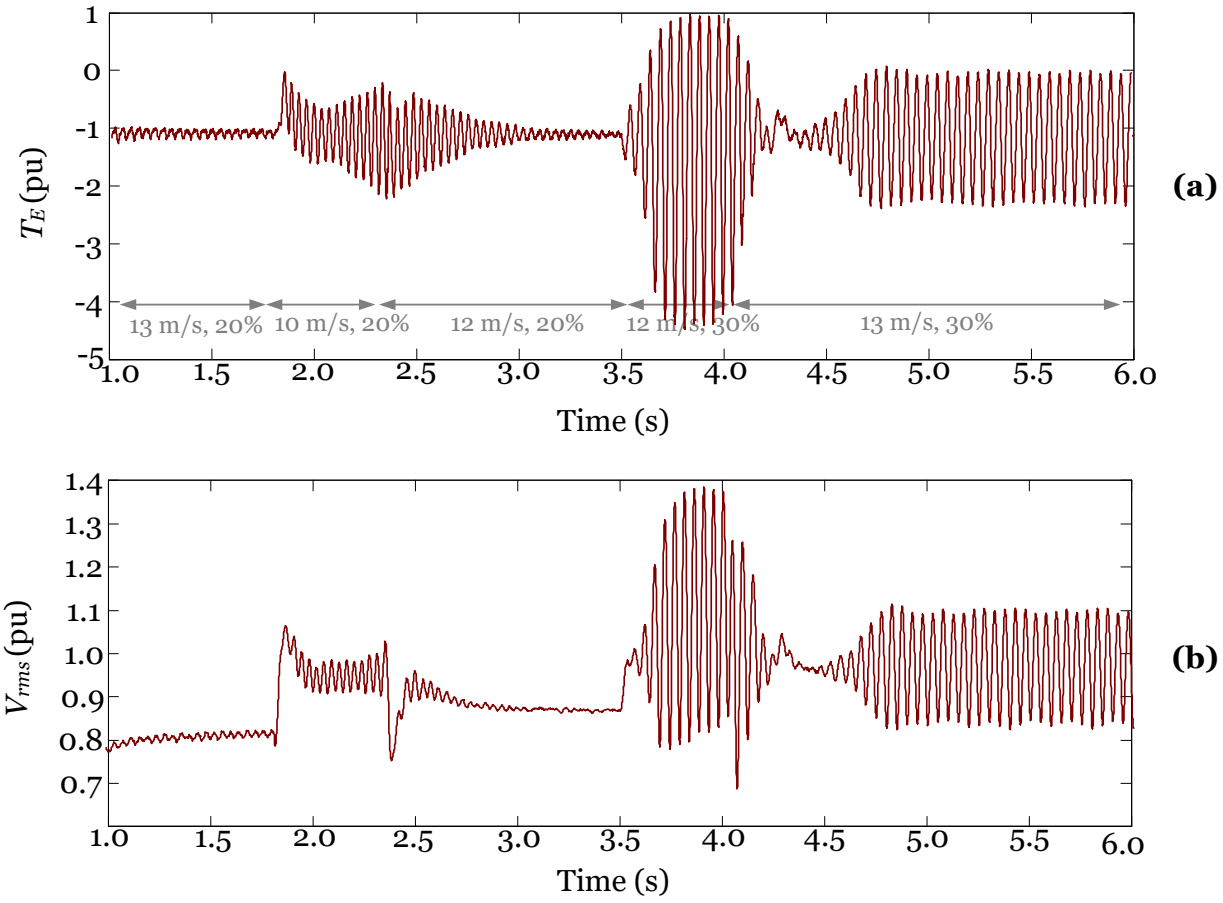

Figure 5.16: Response of the wind turbine 4 to the changes in the wind speed and the compensation level; (a) electric torque of DFIG; (b) RMS voltage of PCC.

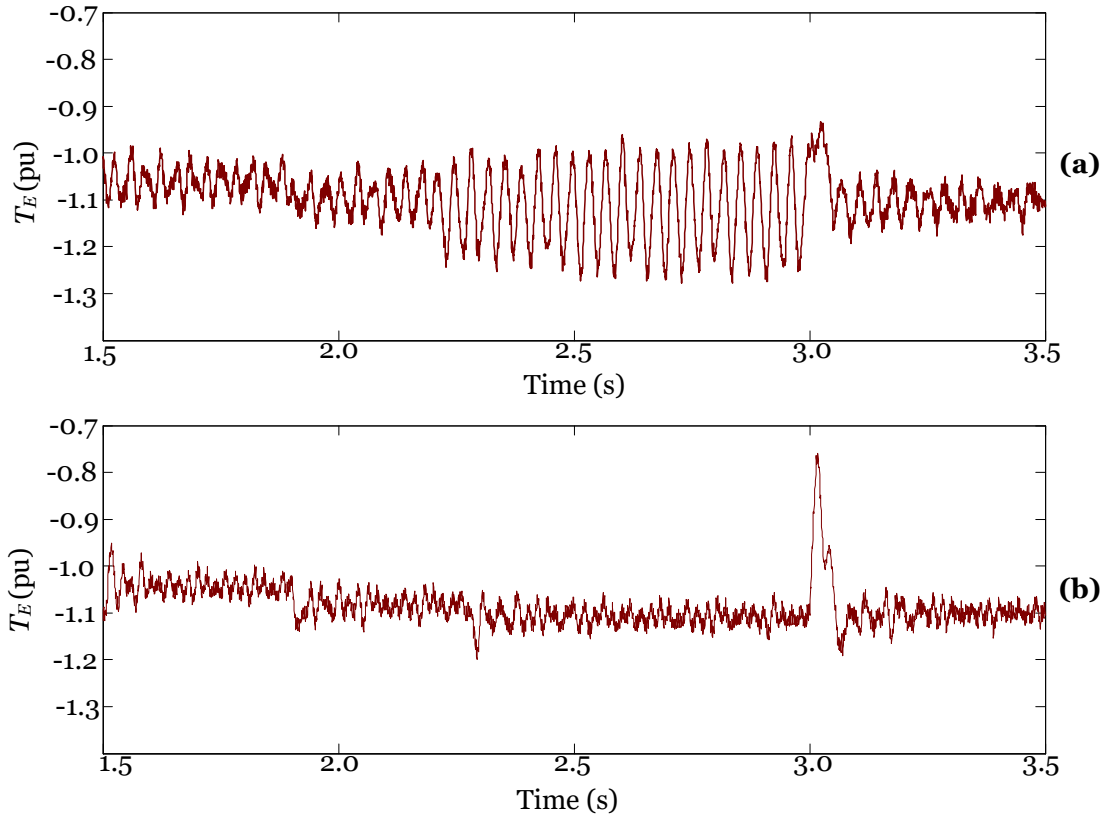

Figure 5.17: Response of the electric torque of wind turbine 1 to a step changes in the compensation level from 30% to 50% at time $t = 2\,\mathrm{s}$. The compensation level is returned to 30% at $t = 3\,\mathrm{s}$; (a) without the proposed controller; (b) with the proposed controller.

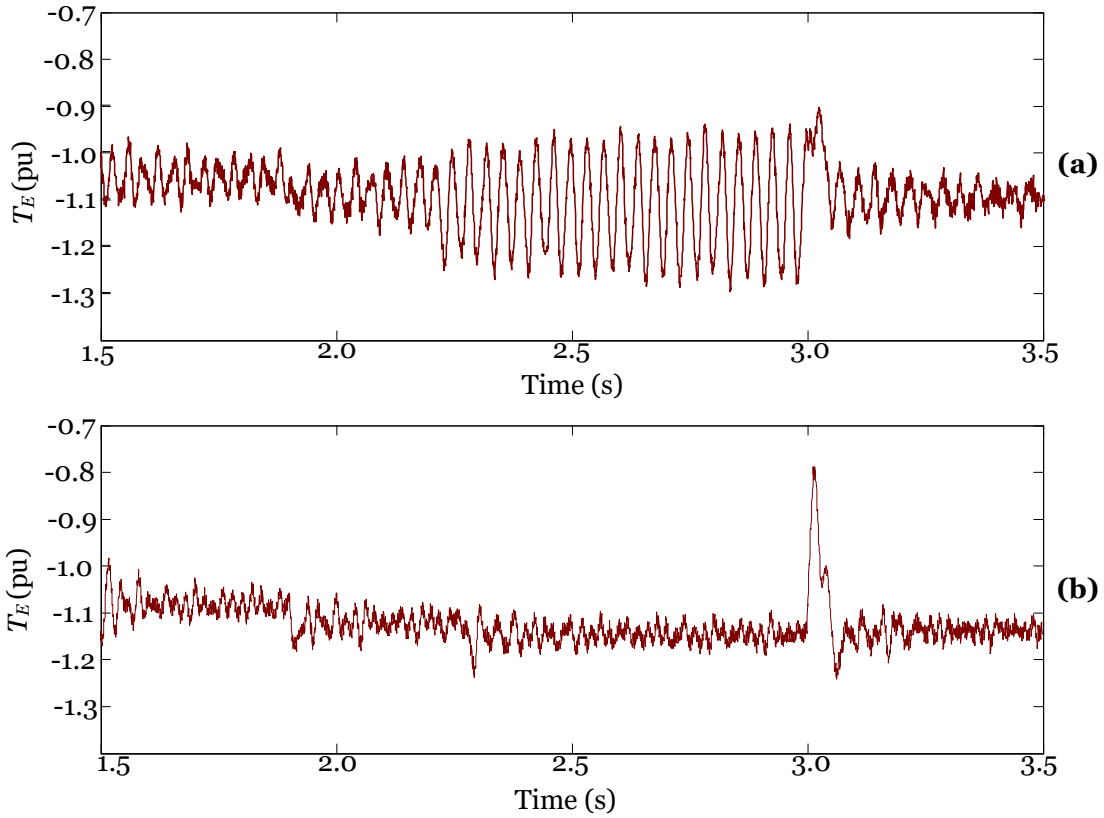

Figure 5.18: Response of the electric torque of wind turbine 2 to a step changes in the compensation level from 30% to 50% at time $t = 2\,\mathrm{s}$. The compensation level is returned to 30% at $t = 3\,\mathrm{s}$; (a) without the proposed controller; (b) with the proposed controller.

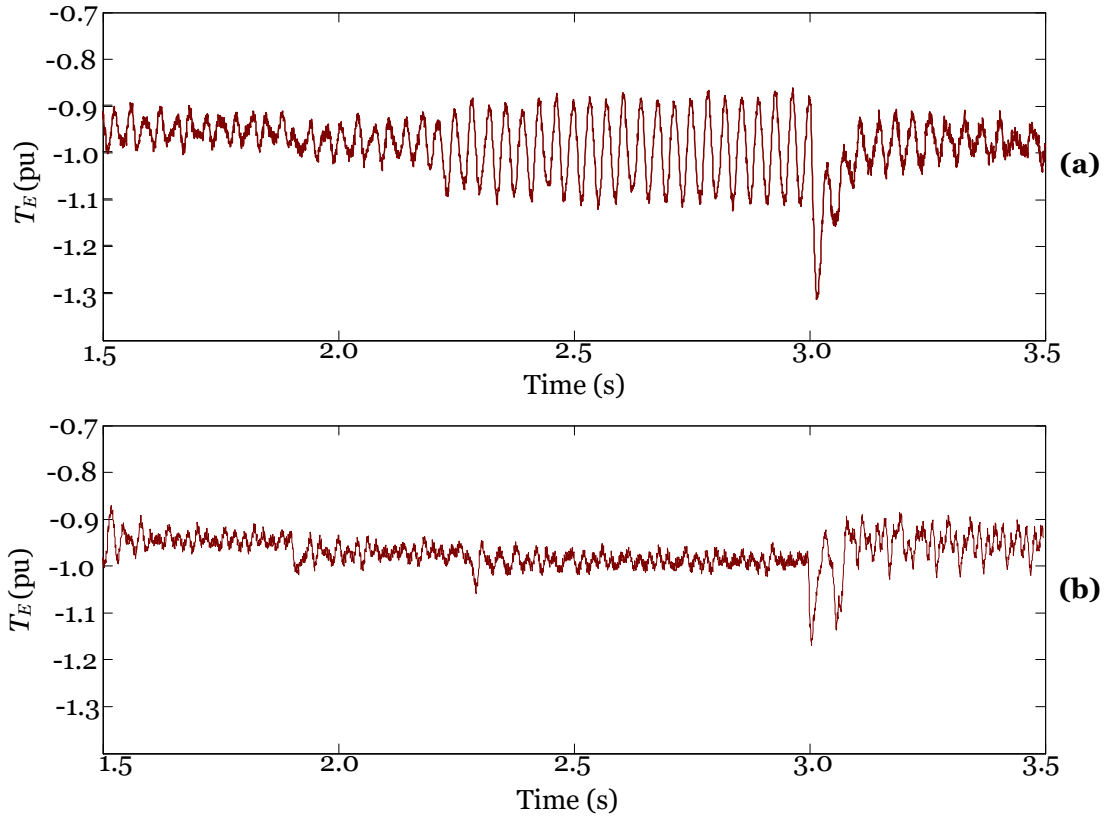

Figure 5.19: Response of the electric torque of wind turbines 3 and 4 to a step changes in the compensation level from 30% to 50% at time $t = 2\,\mathrm{s}$. The compensation level is returned to 30% at $t = 3\,\mathrm{s}$; (a) without the proposed controller; (b) with the proposed controller.

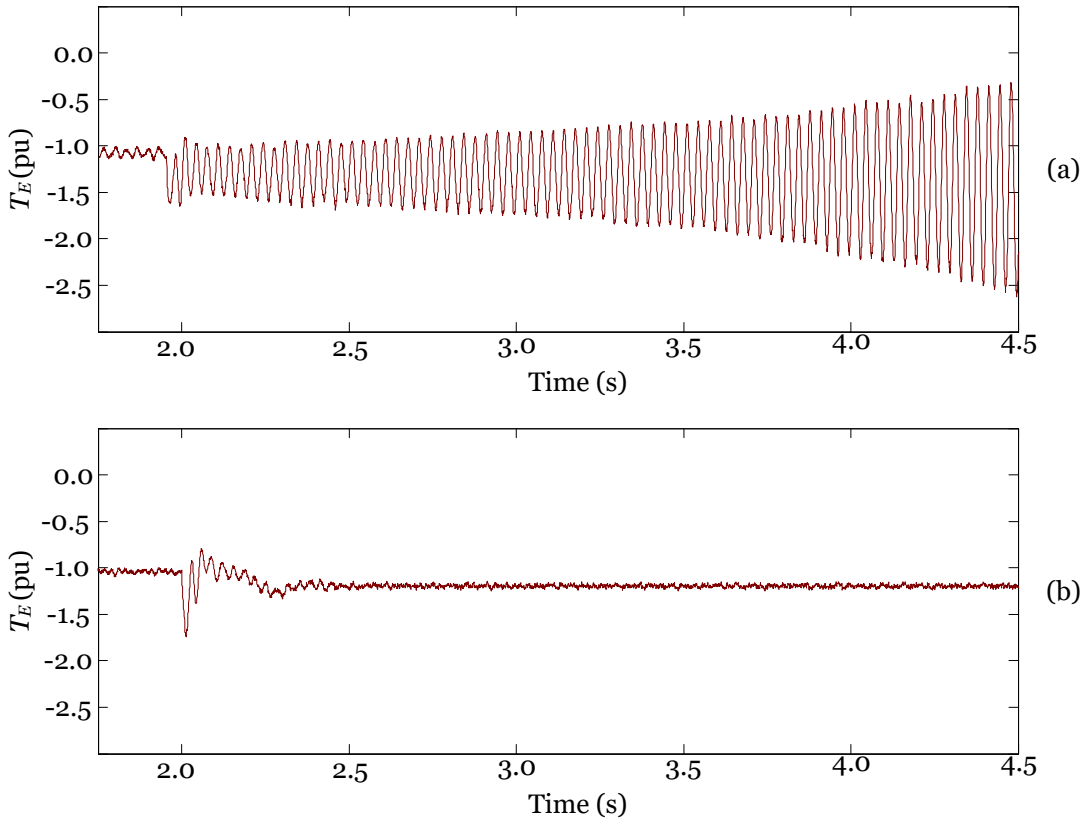

Figure 5.20: Response of the electric torque of wind turbine 1 to a step change in the wind speed of wind turbines 3 and 4 from 10 m/s to 7 m/s at time $t = 2\,\text{s}$; (a) without the proposed controller; (b) with the proposed controller.

It can be seen that wind turbines without the MMAC controllers show an oscillatory behavior to the changes in the compensation level. However, when the MMAC controllers are added to the control loops of the wind turbines, they remain stable after $t = 2\,\text{s}$. This case study shows that the proposed supplementary controller can effectively improve the transient response of a nonaggregated wind system.

5.2.2 Step Change in the Wind Speed

This case study evaluates the stability of the study system for a change in the wind speed of wind turbines in a nonaggregated wind system. Figs. 5.20–5.22(a) and (b) show the response of the electric torque of wind turbines 1–4 to a step change in the wind speed of wind turbines 3 and 4 from 10 m/s to 7 m/s at time $t = 2\,\text{s}$ with and without the MMAC-based supplementary controller.

It can be seen that wind turbines without the MMAC controllers become unstable when the changes occur in the wind speed of the wind turbines 3 and 4. However, when the MMAC controllers are added to the control loops of the wind turbines, they remain stable after $t = 2\,\text{s}$. This case study shows that the proposed supplementary controller can effectively improve the transient response of a nonaggregated wind system.

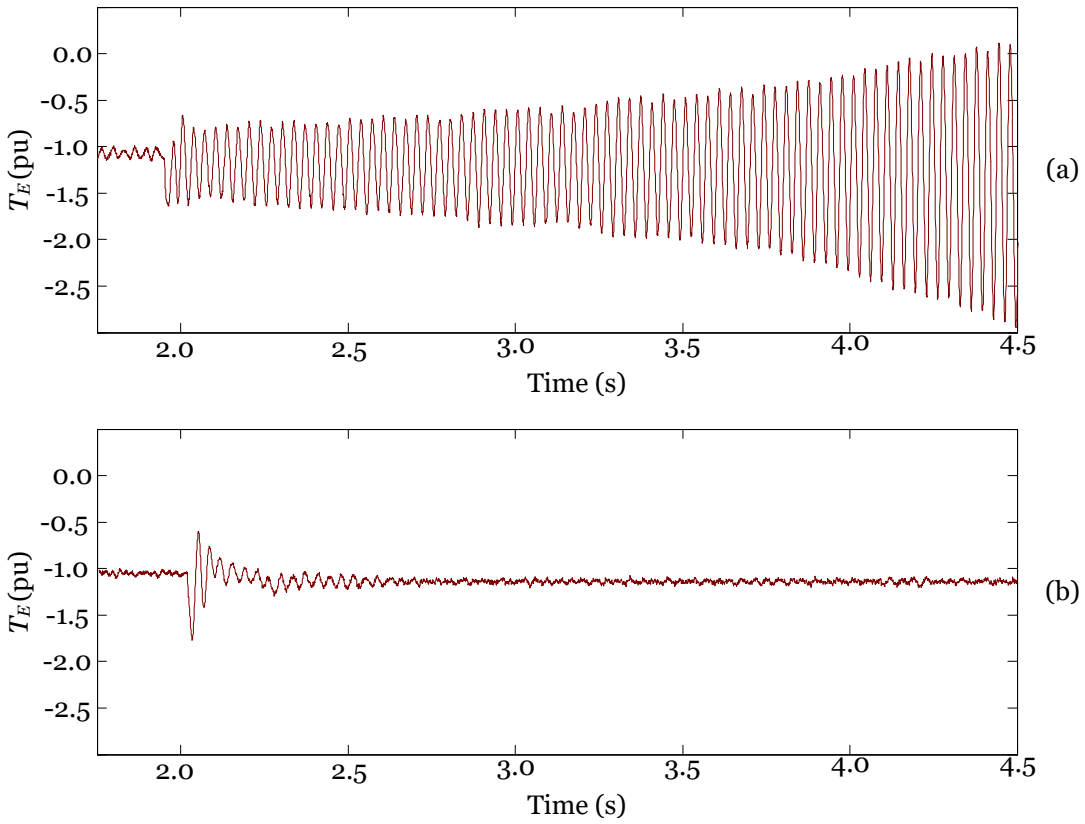

Figure 5.21: Response of the electric torque of wind turbine 2 to a step change in the wind speed of wind turbines 3 and 4 from 10 m/s to 7 m/s at time $t = 2\,\mathrm{s}$; (a) without the proposed controller; (b) with the proposed controller.

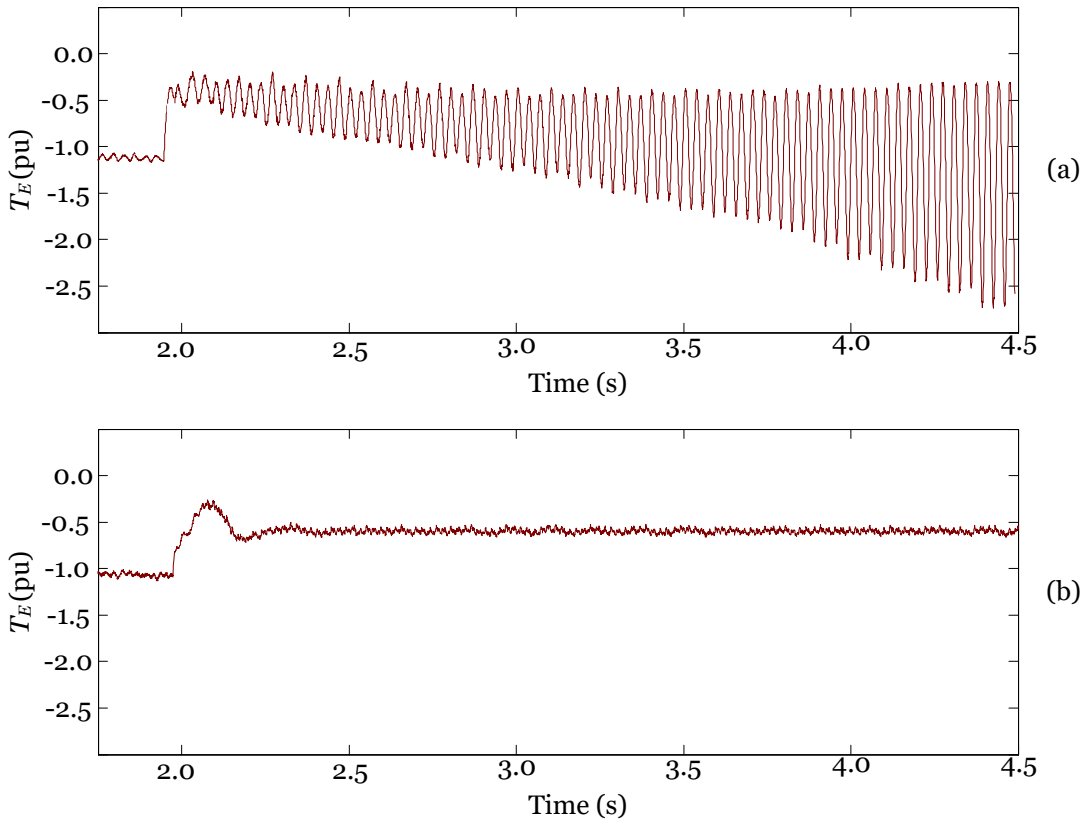

Figure 5.22: Response of the electric torque of wind turbines 3 and 4 to a step change in the wind speed of wind turbines 3 and 4 from 10 m/s to 7 m/s at time $t = 2\,\mathrm{s}$; (a) without the proposed controller; (b) with the proposed controller.

6. Conclusion

Penetration of renewable energy resources into the power grid has increased significantly. SSR is one of the major issues related to integration of wind energy in the power system and it can cause damage or failure of the power system equipment.

An adaptive supplementary controller using the MMAC approach is proposed to mitigate subsynchronous oscillations in a Type III-based wind system. The proposed supplementary controller is a two-level control approach and can operate in a wide range of the operating conditions.

A systematic approach is introduced for simultaneous coordination of parameters of the proposed supplementary controllers in a nonaggregated wind system. The aims of the coordination approach are to stabilize system by moving the unstable modes to the left-hand side and minimize the controllers gain values. The simulation results show the effectiveness of the proposed supplementary controller and the coordination algorithm to mitigate the subsynchronous oscillations in a nonaggregated wind system under a wide range of the operating conditions.

References

[1] M. Singh and S. Santoso, "Dynamic models for wind turbines and wind power plants," *National Renewable Energy Laboratory*, Rep. NREL/SR-5500-52780, May 2011.

[2] R. Hankey, "Electric power monthly," *Rep. U.S. Department of Energy, Energy Information Administration*, Dec. 2017.

[3] S. Lindenberg, B. Smith, K. O. Dell, and E. DeMeo, "20% wind energy by 2030: Increasing wind energy contribution to U.S. electricity supply," *Tech. Rep. U.S. Department Energy*, Rep. DOE/GO-102008-2567, Jul. 2008.

[4] E. Muljadi, C. P. Butterfield, B. Parsons, and A. Ellis, "Effect of variable speed wind turbine generator on stability of a weak grid," *IEEE Trans. Energy Convers.*, vol. 22, no. 1, pp. 29–36, Mar. 2007.

[5] L. Fan, R. Kavasseri, Z. L. Miao, and C. Zhu, "Modeling of DFIG-based wind farms for SSR analysis," *IEEE Trans. Power Del.*, vol. 25, no. 4, pp. 2073–2082, Oct. 2010.

[6] H. A. Mohammadpour and E. Santi, "SSR damping controller design and optimal placement in rotor-side and grid-side converters of series-compensated DFIG-based wind farm," vol. 6, no. 2, pp. 388–399, Apr. 2015.

[7] A. E. Leon and J. A. Solsona, "Sub-synchronous interaction damping control for DFIG wind turbines," vol. 30, no. 1, pp. 419–428, Jan. 2015.

[8] K. Narendra, D. Fedirchuk, R. Midence, N. Zhang, A. Mulawarman, P. Mysore, and V. Sood, "New microprocessor based relay to monitor and protect power systems against sub-harmonics," in *IEEE Electr. Power Energy Conf.*, Winnipeg, Canada, Oct. 2011.

[9] M. S. El-Moursi, B. Bak-Jensen, and M. H. Abdel-Rahman, "Novel STATCOM controller for mitigating SSR and damping power system oscillations in a series compensated wind park," *IEEE Trans. Power Electron.*, vol. 25, no. 2, pp. 429–441, Feb. 2010.

[10] A. Moharana, R. K. Varma, and R. Seethapathy, "SSR alleviation by STATCOM in induction-generator-based wind farm connected to series compensated line," *IEEE Trans. Sustain. Energy*, vol. 5, no. 3, pp. 947–957, Jul. 2014.

[11] U. Karaagac, S. O. Faried, J. Mahseredjian, and A. A. Edris, "Coordinated control of wind energy conversion systems for mitigating subsynchronous interaction in DFIG-based wind farms," *IEEE Trans. Smart Grid*, vol. 5, no. 5, pp. 2440–2449, Sept. 2014.

[12] A. E. Leon, "Integration of dfig-based wind farms into series-compensated transmission systems," vol. 7, no. 2, pp. 451–460, Apr. 2016.

[13] L. Piyasinghe, Z. Miao, J. Khazaei, and L. Fan, "Impedance model-based SSR analysis for TCSC compensated type-3 wind energy delivery systems," *IEEE Trans. Sustain. Energy*, vol. 6, no. 1, pp. 179–187, Jan. 2015.

[14] W. Chen, X. Xie, D. Wang, H. Liu, and H. Liu, "Probabilistic stability analysis of subsynchronous resonance for series-compensated DFIG-based wind farms," *IEEE Trans. Sustain. Energy*, vol. 9, no. 1, pp. 400–409, Jan. 2018.

[15] J. Danie, C. Han, S. Hutchinson, R. Koessler, D. Martin, G. Shen, and W. Wong, "ERCOT CREZ reactive power compensation study," *ABB Inc., Power Systems Division, Grid Systems Consulting*, 2010, E3800-PR-00.

[16] L. H. Hansen, P. H. Madsen, F. Blaabjerg, H. C. Christensen, U. Lindhard, and K. Eskildsen, "Generators and power electronics technology for wind turbines," in *IEEE Annu. Conf. Ind. Electron. Soc. (IECON)*, vol. 3, Denver, CO, Dec. 2001, pp. 2000–2005.

[17] J. A. Baroudi, V. Dinavahi, and A. M. Knight, "A review of power converter topologies for wind generators," *Renewable Energy*, vol. 32, no. 14, pp. 2369–2385, Nov. 2007.

[18] C. V. Hernandez, T. Telsnig, and A. V. Pradas, "JRC wind energy status report - 2016 edition," *Rep. Joint Research Center*, Rep. EUR 28530 EN 2017.

[19] Y. Lei, A. Mullane, G. Lightbody, and R. Yacamini, "Modeling of the wind turbine with a doubly fed induction generator for grid integration studies," *IEEE Trans. Energy Convers*, vol. 21, no. 1, pp. 257–264, Mar. 2006.

[20] S. M. Muyeen, M. H. Ali, R. Takahashi, T. Murata, J. Tamura, Y. Tomaki, A. Sakahara, and E. Sasano, "Transient stability analysis of grid connected wind turbine generator system considering multi-mass shaft modeling," *Electric Power Components and Systems*, vol. 34, no. 10, pp. 1121–1138, 2006.

[21] H. A. Mohammadpour, M. M. Islam, E. Santi, and Y. J. Shin, "SSR damping in fixed-speed wind farms using series FACTS controllers," *IEEE Trans. Power Del.*, vol. 31, no. 1, pp. 76–86, Feb. 2016.

[22] L. Xu and Y. Wang, "Dynamic modeling and control of DFIG-based wind turbines under unbalanced network conditions," vol. 22, no. 1, pp. 314–323, Feb. 2007.

[23] L. Trilla, O. Gomis-Bellmunt, A. Junyent-Ferre, M. Mata, J. S. Navarro, and A. Sudria-Andreu, "Modeling and validation of DFIG 3-MW wind turbine using field test data of balanced and unbalanced voltage sags," *IEEE Trans. Sustain. Energy*, vol. 2, no. 4, pp. 509–519, Oct. 2011.

[24] C. Schauder and H. Mehta, "Vector analysis and control of advanced static var compensators," *IEE Proc. C - Gen. Transm. Dist.*, vol. 140, no. 4, pp. 299–306, Jul. 1993.

[25] L. P. Kunjumuhammed, B. C. Pal, C. Oates, and K. J. Dyke, "Electrical oscillations in wind farm systems: Analysis and insight based on detailed modeling," *IEEE Trans. Sustain. Energy*, vol. 7, no. 1, pp. 51–62, Jan. 2016.

[26] F. Mei and B. Pal, "Modal analysis of grid-connected doubly fed induction generators," *IEEE Trans. Energy Convers*, vol. 22, no. 3, pp. 728–736, Sept. 2007.

[27] B. Pal and B. Chaudhuri, *Robust Control in Power Systems*. New York, USA: Springer US, 2005.

[28] M. Huang, X. Wang, and Z. Wang, "Multiple model adaptive control for a class of linear-bounded nonlinear systems," *IEEE Trans. Autom. Control*, vol. 60, no. 1, pp. 271–276, Jan. 2015.

[29] M. S. El-Moursi, B. Bak-Jensen, and M. H. Abdel-Rahman, "Novel STATCOM controller for mitigating SSR and damping power system oscillations in a series compensated wind park," *IEEE Trans. Power Electron.*, vol. 25, no. 2, pp. 429–441, Feb. 2010.

[30] K. D. Schott and B. W. Bequette, *Multiple Model Adaptive Control (MMAC)*. Dordrecht: Springer Netherlands, 1998, pp. 33–57.

[31] L. Ozkan and M. V. Kothare, "Stability analysis of a multi-model predictive control algorithm with application to control of chemical reactors," *J. Process Control*, vol. 16, no. 2, pp. 81–90, Jun. 2006.

[32] K. S. Narendra and J. Balakrishnan, "Improving transient response of adaptive control systems using multiple models and switching," *IEEE Trans. Autom. Control*, vol. 39, no. 9, pp. 1861–1866, Sept. 1994.

[33] W. Chen and B. D. O. Anderson, "A combined multiple model adaptive control scheme and its application to nonlinear systems with nonlinear parameterization," *IEEE Trans. Autom. Control*, vol. 57, no. 7, pp. 1778–1782, Jul. 2012.

[34] L. Xu and S. Ahmed-Zaid, "Tuning of power system controllers using symbolic eigensensitivity analysis and linear programming," *IEEE Trans. Power Syst.*, vol. 10, no. 1, pp. 314–322, Feb. 1995.

[35] P. Pourbeik and M. J. Gibbard, "Simultaneous coordination of power system stabilizers and FACTS device stabilizers in a multimachine power system for enhancing dynamic performance," *IEEE Trans. Power Syst.*, vol. 13, no. 2, pp. 473–479, May 1998.